# The Los Alamos Trapped Ion Quantum Computer Experiment

by

R. J. Hughes [1][1], D. F. V. James [4], J. J. Gomez [3], M. S. Gulley [3], M. H. Holzscheiter [1], P. G. Kwiat [1], S. K. Lamoreaux [1], C. G. Peterson [1], V. D. Sandberg [1], M. M. Schauer [2], C. M. Simmons [1], C. E. Thorburn [1][2], D. Tupa [1], P. Z. Wang [1][3], A. G. White [1].

[1] Physics Division P-23, Mail Stop H-803,
[2] Physics Division P-24, Mail Stop E-526,
[3] Physics Division P-25, Mail Stop H-846,
[4] Theoretical Division T-4, Mail Stop B-268,
University of California
Los Alamos National Laboratory
Los Alamos, NM87545, USA

submitted to *Fortschritte der Physik*
26 August 1997

## Abstract

The development and theory of an experiment to investigate quantum computation with trapped calcium ions is described. The ion trap, laser and ion requirements are determined, and the parameters required for quantum logic operations as well as simple quantum factoring are described.

PACS numbers: 32.80.Qk, 42.50.Vk, 89.80.+h
LA-UR-97-3301

[1]Address correspondence to Dr. Richard J. Hughes, Physics Division P-23, Mail Stop H-803, Los Alamos National Laboratory, Los Alamos NM 87545, USA. Email hughes@lanl.gov. More information can be obtained at our website: http://p23.lanl.gov/Quantum/quantum.html
[2]Current address: Engineering Sciences and Applications Division ESA-MT, MS C-914, Los Alamos National Laboratory
[3]Permanent address: Physics Dept., Cornell University, Ithaca, N.Y.

# 1 Introduction

In the early 1980's, various authors started to investigate the generalization of information theory concepts to allow the representation of information by quantum states. The introduction into computation of *quantum* physical concepts, in particular the superposition principle, opened up the possibility of new capabilities, such as quantum cryptography [1], that have no classical counterparts. One of the most intriguing of these new ideas is quantum computation, first proposed by Benioff [2]. Subsequently Feynman [3] suggested that quantum computation might be more powerful than classical computation. This notion gained further credence through the work of Deutsch who introduced the idea of quantum parallelism to describe the ability of a quantum computer to compute with quantum superpositions of numbers [4]. Deutsch and Josza illustrated this power of quantum computation with an Oracle problem [5]. However, until 1994 quantum computation was an essentially academic endeavor because there were no quantum algorithms that exploited this power to solve interesting computational problems, and because no realistic hardware capable of performing quantum computations had been envisioned. But then, building on earlier work of Simon [6], Shor discovered quantum algorithms for efficient solution of two problems that are at the heart of the security of much of modern public key cryptography: integer factorization and the discrete logarithm problem [7, 8]. Later in 1994 Cirac and Zoller proposed that quantum computational hardware could be realized using known techniques in the laser manipulation of trapped ions [9]. Since then interest in quantum computation has grown dramatically, with several groups, including our own, now pursuing trapped ion and other quantum computation experiments.

Since 1994 remarkable progress has been made: a single quantum logic gate has been demonstrated with trapped ions [10]; quantum error correction schemes have been invented [11, 12]; and quantum algorithms for solving new problems have been discovered [13, 14, 15, 16]. In this paper we will review the subject of quantum computation and our development of an experiment using trapped calcium ions. Also, we will explore the potential of this technology and determine whether the future obstacles to progress will be fundamental or technical.

The remainder of this paper is organized as follows. In section 2, the essential principles of quantum computation are introduced. Section 3 briefly describes the potential for efficiently factoring large numbers with a quantum computer. In section 4, we discuss various quantum computational hardware ideas; the trapped ion proposal is then described in detail in section 5. The experiment we are undertaking to realize

such a trapped ion quantum computer is described in section 6, and the last section summarizes our conclusions.

## 2 The Principles of Quantum Computation

The principles of quantum computation have been discussed in detail elsewhere (see for example [8, 17]) so we shall only give a very brief introduction here. The essential idea of quantum computation is to represent binary numbers using a collection of two-level quantum systems. We will use the notation $\{|0\rangle, |1\rangle\}$ to denote the states of a single two-level quantum system, known as a quantum bit or *qubit*.

With multiple qubits the number of degrees of freedom in the system rapidly increases: the Hilbert space describing the state of a system containing $N$ qubits has $2^N$ dimensions. It is possible to use such a system to represent a number, $x$, between 0 and $\left(2^N - 1\right)$, as the state

$$|x\rangle \equiv \prod_{i=0}^{N-1} |x_i\rangle_i, \tag{2.1}$$

where $x = \sum_{i=0}^{N-1} x_i 2^i$, and $x_i$ is the $i$th binary digit of $x$. Thus, for example, the decimal number 11, which is written as 1011 in binary, would be represented by four qubits in the state $|1\rangle_3|0\rangle_2|1\rangle_1|1\rangle_0$, which is more conveniently written in the short-hand notation $|1011\rangle$.

To perform computations, we need to be able to perform certain unitary operations that act on sets of qubits, known as *quantum logic gates*. Because quantum interactions are reversible, the underlying logic of a quantum computer must itself be reversible. Fortunately, it is already known that arbitrary Boolean operations can be constructed reversibly [18], [19].

An example of a reversible logic operation is the $NOT$ operation on a single qubit:

$$NOT : |b\rangle \rightarrow |\bar{b}\rangle. \tag{2.2}$$

Arithmetic operations require logic operations between two or more qubits. For example, in the controlled-NOT operation on two qubits

$$CNOT : |c\rangle|t\rangle \rightarrow |c\rangle|t \oplus c\rangle, \tag{2.3}$$

a target qubit, t, is flipped in value when a control qubit, c, has the value 1, but is unchanged when the control has the value 0. The symbol $\oplus$ denotes addition modulo 2, defined by the following truth table:

| a | b | a $\oplus$ b |
|---|---|---|
| 0 | 0 | 0 |
| 0 | 1 | 1 |
| 1 | 0 | 1 |
| 1 | 1 | 0 |

.

A second application of the CNOT gate returns the state to its starting value.

Another reversible logic gate used in quantum computing is the three-bit controlled controlled-NOT (or Toffoli gate):

$$CCNOT : |c_1\rangle|c_2\rangle|t\rangle \rightarrow |c_1\rangle|c_2\rangle|\left(c_1 \wedge c_2\right) \oplus t\rangle, \tag{2.4}$$

where $\wedge$ denotes the logical AND defined by the following truth table:

| a | b | a $\wedge$ b |
|---|---|---|
| 0 | 0 | 0 |
| 0 | 1 | 0 |
| 1 | 0 | 0 |
| 1 | 1 | 1 |

.

Using the Toffoli and CNOT gates it is possible to construct a simple binary adder:

$$ADD\left(|a\rangle, |b\rangle, |0\rangle\right) = CNOT_{1,2}\left(CCNOT\left(|a\rangle, |b\rangle, |0\rangle\right)\right) = |a\rangle|a \oplus b\rangle|a \wedge b\rangle \tag{2.5}$$

which places the sum modulo 2 of the first and second inputs (reading left to right) onto the second output, and the carry bit (originally reading 0) into the third output qubit. (Here, the CNOT-operation on three qubits is defined as: $CNOT_{1,2} : |a\rangle|b\rangle|c\rangle \rightarrow |a\rangle|a \oplus b\rangle|c\rangle$ .) With these *universal* quantum logic gates, arbitrary arithmetic functions can be formed.

So far our discussion has not revealed any particular power associated with quantum computation. Indeed, it is clear that the physical requirement of logical reversiblity leads to extra information (relative to conventional computation) being carried forward. This extra information, which allows the input of a logical operation to be determined from the output, imposes additional memory requirements on quantum computation. Nevertheless, it is known that the peculiarly quantum concepts of superposition and interference can be utilized to provide a much more efficient solution of certain problems than is possible on any conventional computer. We consider computations with superpositions of numbers first. A unitary operation on a single qubit can be written as

$$\hat{V}\left(k, \phi\right) : \left\{ \begin{array}{l} |0\rangle \\ |1\rangle \end{array} \right\} \rightarrow \left\{ \begin{array}{l} \cos\left(\frac{k\pi}{2}\right)|0\rangle - i\exp\left(i\phi\right)\sin\left(\frac{k\pi}{2}\right)|1\rangle \\ \cos\left(\frac{k\pi}{2}\right)|1\rangle - i\exp\left(-i\phi\right)\sin\left(\frac{k\pi}{2}\right)|0\rangle \end{array} \right\}. \tag{2.6}$$

For example, $\hat{V}\left(1/2, \pi/2\right) : |0\rangle \rightarrow 2^{-1/2}\left(|0\rangle + |1\rangle\right)$ , is an equally-weighted superposition of both qubit states. Now, starting with an $L$-qubit register in the state $|0\rangle \equiv \prod_{i=0}^{L-1} |0\rangle_i$ , and acting on each qubit with $\hat{V}\left(1/2, \pi/2\right)$ produces a coherent superposition of all $2^L$ possible numbers:

$$|0\rangle \rightarrow 2^{-L/2} \prod_{i=0}^{L-1} \left(|0\rangle_i + |1\rangle_i\right) = 2^{-L/2} \sum_{a=0}^{2^L-1} |a\rangle. \tag{2.7}$$

Thus, in a sense the memory of a quantum computer is exponentially large. Now the quantum register state above is a product state, whereas a more typical superposition state of the register will be an entangled state (i.e. a state which cannot be written as a simple tensor product of basis states). Such states can be produced with the aid of quantum logic operations. For example, an entangled state of two qubits can be produced from an initial product state:

$$CNOT : 2^{-1/2}\left(|0\rangle + |1\rangle\right)|0\rangle \rightarrow 2^{-1/2}\left(|0\rangle|0\rangle + |1\rangle|1\rangle\right). \tag{2.8}$$

Entangled states are required during typical quantum computations (and it is the existence of such entanglements that distinguish a quantum computer from a classical computer), but because of their non-classical properties the CNOT operation is extremely difficult to construct in a physical system.

Thus far we have seen the power of quantum memory. Now we explore the power of actual quantum computations. Let us suppose that we have determined the sequence of quantum gates required to evaluate (reversibly) the value of some function, F, for an arbitrary input, a:

$$\hat{F} : |a\rangle|0\rangle \rightarrow |a\rangle|F\left(a\right)\rangle, \tag{2.9}$$

where the argument is held in the left register, and the right register is to hold the function value. We might as easily have started with the left register in an equally-weighted superposition of all values, and applied the same sequence of logic gates:

$$\hat{F} : \sum_{a=0}^{2^L-1} |a\rangle|0\rangle \rightarrow \sum_{a=0}^{2^L-1} |a\rangle|F\left(a\right)\rangle, \tag{2.10}$$

evaluating all $2^L$ function values in one step. (Recall that the initial state of the left register can be created from the $|0\rangle$ state with only $L$-single qubit unitary operations.) If we were only interested in the function values we would now have to repeat the creation of this state $O(2^L)$ times, and measure the right register each time in order to determine the values. Obviously, for this type of problem quantum computation

offers no advantages, but if we were instead interested in some joint property shared by all the function values, such as the function's period, we could now perform a quantum Fourier transform (QFT) operation on the left register to determine the period efficiently. The point is that particular function values in the right register are associated with sequences of values in the left register that reflect the period. The QFT, which is given by the following formula

$$|a\rangle \rightarrow 2^{-\frac{L}{2}} \sum_{c=0}^{2^L-1} \exp\left(i\frac{a.c}{2^L}\right)|c\rangle, \tag{2.11}$$

regroups these sequences to produce constructive interference at values corresponding to periods of the sequence. Furthermore, the QFT itself can be constructed using only $O(L^2)$ quantum gates, whereas a conventional discrete Fourier transform requires $O(L2^L)$ operations for a $L$-bit input register. For problems that can be reduced to determining the period of a function, quantum computation may offer a more efficient solution than conventional computation. All known quantum algorithms to solve interesting problems use either the QFT or one of its variants, such as the quantum Hadamard transformation.

# 3 Quantum Factoring

The power of quantum computing can be illustrated with the example of Shor's algorithm for integer factorization. According to the fundamental theorem of arithmetic, every integer has a unique expression as a product of primes. Most modern factoring algorithms use as their starting point the Legendre congruence: given a composite integer, N, which we want to factor, the congruence

$$y^2 = 1 \bmod (N) \tag{3.1}$$

has non-trivial solutions, $y = \pm a \bmod (N)$, in addition to the trivial solutions, $y = \pm 1 \bmod (N)$. If a non-trivial solution, $a$, can be found, it can be used to find a factor of N, because the congruence

$$(a+1)(a-1) = 0 \bmod (N) \tag{3.2}$$

implies that the factors of $N$ are distributed between the two parentheses. Therefore, the greatest common divisor ($gcd$)

$$gcd(a \pm 1, N) = \text{factor of N}, \tag{3.3}$$

which can be found using Euclid's algorithm, gives a factor of $N$. The problem of integer factorization can therefore be reduced to finding a suitable a.

Shor's algorithm for finding factors using a quantum computer starts by using a classical computer to find an integer x which shares no common factors other than 1 with N:

$$(x, N) = 1 \tag{3.4}$$

Once a value of $x$ is known the function given by the following expression can be defined:

$$f_x(z) = x^z \bmod (N),\ z = 0, 1, 2, \cdots, N^2 - 1. \tag{3.5}$$

This function will be periodic, with some period r, (known as the order of $x \bmod (N)$). Mathematically, for some r,

$$f_x(z + r) = f_x(z), \tag{3.6}$$

and hence

$$x^r = 1 \bmod (N). \tag{3.7}$$

Thus, if r is even $a = x^{r/2} \bmod (N)$ is a candidate solution of Legendre's congruence and hence allows factorization of N. (There are some technicalities about the choice of the upper limit to the domain of $f_x$ and the classical post-processing required to deduce r from the quantum part of the algorithm.)

Shor's algorithm requires a $2\log_2 N$ bit left quantum register to hold the argument z, and an $l = \log_2 N$ bit right register to hold the value of the function f:

$$|\psi\rangle = \prod_{i=0}^{2l-1} |0\rangle_{iL} \prod_{j=0}^{l-1} |0\rangle_{jR} \equiv |0\rangle_L |0\rangle_R \tag{3.8}$$

where the suffix i (j) denotes the i-th (j-th) qubit of the left (right) register respectively.

Next, the left register is prepared in a superposition of all possible values, $z$, using 2l operations, $\hat{V}(1/2, \pi/2)$, one for each qubit:

$$|\psi\rangle \rightarrow \prod_{i=0}^{2^{2l}-1} \hat{V}_i (1/2, \pi/2) |\psi\rangle = \frac{1}{2^l} \sum_{i=0}^{2l-1} |z\rangle_L |0\rangle_R \equiv |\psi_1\rangle \tag{3.9}$$

In the next step the function $f_x(z)$ is written into the right register:

$$|\psi_1\rangle \rightarrow \frac{1}{2^l} \sum_{i=0}^{2^{2l}-1} |z\rangle_L |f_x(z)\rangle_R \equiv |\psi_2\rangle \tag{3.10}$$

Because the function $f_x$ is an exponential, the computation to build the function can be broken down into repeated multiplications, which can be reduced to repeated

addition, and ultimately represented in terms of the simple adder and similar circuits. The total number of quantum gates required is therefore $O\left(l^3\right)$ and some additional register space (roughly $2l$ qubits) is required for this computation to proceed reversibly. The resulting state has the form

$$|\psi_2\rangle \sim \frac{1}{2^l} \sum_{z_0} \sum_j |z_0 + jr\rangle_L |f_x\left(z_0\right)\rangle_R \tag{3.11}$$

in which sequences of left register states, separated by the period r, are associated with common right register states. At this stage, it is easier to think about making a measurement of the right register, resulting in a particular value $f\left(z_0\right)$ :

$$|\psi_2\rangle \rightarrow |\phi\rangle \sim \sum_j |z_0 + jr\rangle_L. \tag{3.12}$$

Finally, a quantum Fourier transform can be performed on this state after which a measurement is made, resulting in some value $2^{2l}/jr$ for some j. From this result, the order r can be determined, and hence N can be factored. Note that there are some subtleties involved when r does not divide $2^{2l}$ , and also the algorithm must be repeated until an $x$ with an even r is found.

To put Shor's factoring algorithm in perspective, the total number of logic gates, $N_g$ and the total number of qubits $L$ required to factor an $\ell$-bit integer using a version of the algorithm that we have recently developed are [20]:

$$\begin{aligned} N_g &= 24\ell^3 + O(\ell^2) \\ L &= 5\ell + 4. \end{aligned} \tag{3.13}$$

In contrast, the best algorithm for factoring a large integers $N$ using classical computers is the (general) Number Field Sieve (NFS) [21], which runs in an asymptotic heuristic time $T_R$ given by:

$$T_R \sim \exp\left[1.923\ell^{1/3}(\log \ell)^{2/3}\right]. \tag{3.14}$$

The NFS has much faster growth with the number of bits in N than the polynomial growth of the quantum algorithm. The NFS was recently used to factor the 130-digit (430-bit) integer known as RSA130 [22] using approximately 500 MIPS-years of computer time distributed over the Internet. (1 MIPS-year is approximately $3.0 \times 10^{13}$ instructions.) With one hundred machines each rated at 100 MIPS dedicated to this problem we would estimate a factoring time of approximately 18 days. In contrast the quantum factoring algorithm applied to the same integer would require only $\sim 2.0 \times 10^9$

quantum logic gates. If a quantum computer had a clock speed of 100 MHz it would factor this number in only ∼20 seconds. Furthermore, the tremendous efficiency of the quantum computer would become even more pronounced with larger numbers.

# 4 Quantum Computer Technologies

The three essential requirements for quantum computational hardware are: (1) the ability to isolate a set of two-level quantum systems from the environment for long enough to maintain coherence throughout the computation, while at the same time being able to interact with the systems strongly enough to manipulate them into an arbitrary quantum state; (2) a mechanism for performing quantum logic operations: in other words a "quantum bus channel" connecting the various two-level systems in a quantum mechanical manner; and (3) a method for reading out the quantum state of the system at the end of the calculation.

So far the serious proposals for quantum computational hardware fall into five basic categories:

1. Ion traps. In this scheme the quantum data registers consist of internal levels of ions trapped in a linear configuration; the quantum bus channel is realized using the phonon modes of the ions' collective oscillations; and readout is performed by using quantum jumps. This scheme was originally proposed by Cirac and Zoller in 1994 [9], and was used to demonstrate a CNOT gate shortly afterwards [10]. The number of qubits that can be realized using an ion trap is limited by the various decoherence mechanisms, which have been discussed in detail elsewhere [23, 24, 25, 26], and by the onset of instabilities in the linear configuration of the ions [27]. One estimate [23] suggests that computations involving 47 qubits and $4.0 \times 10^5$ operations may be possible with trapped Calcium ions before decoherence becomes a serious problem, although this estimate ignores experimental decoherence effects such as ion heating and fluctuations of laser phases, as well as recent advances in the field of quantum error correction. (A variant of this idea using a photon mode of a cavity as the quantum bus bit has also been proposed [28].) Our progress towards realizing a trapped ion quantum computer is the subject of the remainder of this article.

2. Cavity Quantum Electrodynamics (Cavity QED). Here the quantum data register consists of the photon modes of an optical cavity, which are linked to other modes via excitation of, and emission by, an atom passing through the cavity. This scheme is a development of experiments in cavity quantum electrodynamics, and it has been used

successfully to realize quantum gates, although scaling up to more than 2 or 3 qubits will probably be very difficult [29, 30]. A related *all photon* cavity QED realization has been proposed [31].

3. Nuclear Magnetic Resonance (NMR). The orientation of spin-1/2 nuclei in a molecule form the data register, and the spin-spin interactions provide the quantum bus channel. The states of the spins can be altered by applying a radio-frequency magnetic field and readout is performed by measuring the magnetization of bulk samples, a procedure which can only measure an *ensemble average* of the quantum state populations. There are considerable subtleties associated with preparation of the initial states as well as with the readout; for this reason, the NMR scheme has been called "*ensemble quantum computing*" [32] (see also [33]). This method has been used to realize experimental quantum gates involving two and three qubits [34], however because the signal falls exponentially with the number of qubits, the ability to scale up to large numbers of qubits seems to be problematic [35]: the sources cited above give estimates of the largest number of qubits that can be realized with NMR computers that vary from 6 to 20.

Similar concepts involving electron spins [36], the use of atomic force microscopy to manipulate nuclear spins [37] and the interactions between electron and nuclear spins in the quantum Hall regime [38] have been proposed.

4. Superconducting Quantum Interference Devices (SQUIDS). In this proposed realization, which is still being developed and has not yet been used to realize a quantum logic gate, the quantization of flux in a superconducting circuit would be exploited to give two level systems [39, 40, 41]. The principal attraction of this proposal is that it is a solid state device, and so if it can be made to work with a small number of qubits, scaling up to large numbers of qubits should be relatively straightforward because the technology for making miniaturized solid state devices containing a very large number of computing elements already exists. However, solid state devices will also have their drawbacks, in that they will be strongly coupled to a complex environment, so decoherence may become an insurmountable problem.

5. Quantum Dots. Quantum dots are regions of artificial inhomogeneity in a crystal, which can be placed in a controlled manner. They can be used to trap single electrons, the orientation of whose spin can then be used as to store information [42, 43]. Like the SQUID proposal, this idea has not yet been used to demonstrate a logic gate, but offers the same advantage of being a solid state device.

# 5 Theory of Quantum Computation with Ions in a Linear Trap

We shall now describe in detail the Cirac-Zoller trapped-ion quantum computer concept [9] (see also refs. [44, 45]). In this scheme, illustrated in fig.1, each qubit is the electronic ground state ($|0\rangle$) and a metastable excited state ($|1\rangle$) of an ion, which has been laser cooled to rest in a linear radio-frequency quadrupole ion trap. Computational operations are performed with coherent laser-ion interactions driving Rabi oscillations between the relevant quantum states of the register. At the end of the computation, the results are read out using the quantum jump technique. The principal advantages of the trapped ion scheme are that many of the techniques required to prepare and manipulate quantum states have already been developed for precision spectroscopy work; secondly that the decoherence rates owing to decay of the excited ionic state and heating of the ionic motion can be made small in the virtually perturbation-free (ultra-high vacuum, low electromagnetic noise level) environment of an ion trap; and finally there is an experimentally demonstrated technique, quantum jumps, for reading out the result of a computation with high probability.

The first step that must be accomplished for quantum computation is to prepare an isolated quantum state of several ions in which each ion is spatially localized and cooled to the quantum ground state of its vibrational motion. The techniques employed for trapping and cooling the ions are described in detail below. Operating the trap at low ion densities, Doppler cooling produces a so-called "string-of-pearls" configuration: the ions become arranged in a line and each is localized in a spatial region whose dimensions are very much less than the wavelength of the optical transition. The spacing between adjacent ions can be made conveniently large (30 $\mu$m, say) by striking a balance between their Coulomb repulsion and the axial confining potential. This crystallized structure permits the ions to be addressed by lasers for quantum computation. It has been demonstrated that a single ion can be cooled to its vibrational ground state in an ion trap using resolved sideband cooling in the optical regime [46]. Because we shall employ the quanta of the ions' collective vibrations (i.e. phonons) as a "quantum bus channel" connecting different qubits, these vibrations must initially be in their ground states. However, cooling to the vibrational ground state has yet to be demonstrated for two or more ions. With the ions in their internal and phonon ground states and with the cooling lasers turned off the system is prepared for the actual quantum computation to begin.

## 5.1 Phonon Modes

We shall assume that ions are sufficiently tightly bound in the directions transverse to the trap axis that we need only consider their motion along the axial direction (i.e. the x-axis in fig.1). Suppose that the m-th ion is displaced a small distance $q_m$ from its equilibrium position $x_m^0$. The Lagrangian for the oscillations of the ions about their equilibrium positions is

$$L\left(\dot{q}_m, q_m\right) = \frac{M}{2}\sum_{m=1}^{N}\left(\dot{q}_m\right)^2 - \frac{1}{2}\sum_{n,m=1}^{N} C_{nm} q_n q_m, \tag{5.1}$$

where $N$ is the number of ions, $M$ is the mass of each ion and the coupling matrix $C_{nm}$ is defined by

$$C_{nm} = \left[\frac{\partial^2 V}{\partial x_n \partial x_m}\right]_0, \tag{5.2}$$

where $V$ here stands for the ions' potential energy, and the subscript 0 denotes that the double partial derivative is evaluated at $q_n = q_m = 0$. The potential energy, which consists of two parts, the binding potential due to the trap electrodes and the Coulomb interaction energy between the ions themselves, is given by:

$$V\left(x_m\right) = \sum_{m=1}^{N}\frac{1}{2}M\omega_x^2 x_m(t)^2 + \sum_{\substack{n,m=1\\ m\neq n}}^{N}\frac{e^2}{8\pi\epsilon_0}\frac{1}{\left|x_n(t) - x_m(t)\right|}\ , \tag{5.3}$$

where $x_m(t) = x_m^0 + q_n(t)$ is the position of the m-th ion, $e$ is the charge of the electron (we have assumed that the ions are singly ionized), $\epsilon_0$ is the permittivity of free space and $\omega_x$ is the angular frequency characterizing the the harmonic binding potential. If there were only one ion confined in the trapping potential, then its oscillations would be harmonic with this angular frequency. The elements of the matrix $C_{nm}$ may be calculated by differentiating eq.(5.3) and evaluated using the values for the equilibrium positions of the ions, obtained numerically (see ref. [49]).

The eigenvectors $b_m^{(p)}$ $(p = 1, 2, \ldots N)$ of the matrix $C_{nm}$ are defined by the following formulas:

$$\sum_{n=1}^{N} C_{nm} b_n^{(p)} = \mu_p^2 b_m^{(p)}\ \left(p = 1, \ldots, N\right)\ , \tag{5.4}$$

where $\mu_p^2$ $(p = 1, 2, \ldots N)$ are the eigenvalues (which are always positive). The eigenvectors are assumed to be numbered in order of increasing eigenvalue and to be properly normalized. The first eigenvector (i.e. the eigenvector with the smallest eigenvalue) can be shown to be

$$\mathbf{b}^{(1)} = \frac{1}{\sqrt{N}}\left\{1, 1, \ldots, 1\right\}, \qquad \mu_1 = 1\ . \tag{5.5}$$

The *normal modes* of the ion motion are defined by the formula

$$Q_p(t) = \sum_{m=1}^{N} b_m^{(p)} q_m(t) \ (p = 1, 2, \ldots N) \ . \tag{5.6}$$

The first mode $Q_1(t)$ corresponds to all of the ions oscillating back and forth as if they were rigidly clamped together; this is referred to as the *center of mass* (CM) mode. The second mode $Q_2(t)$ corresponds to each ion oscillating with an amplitude proportional to its equilibrium distance from the trap center. This is called the *breathing mode*. There are a total of $N$ modes altogether.

The Lagrangian for the ion oscillations, eq. (5.1), may be rewritten in terms of these normal modes as follows:

$$L\left(\dot{q}_m, q_m\right) = \frac{M}{2} \sum_{p=1}^{N} \left[\dot{Q}_p^2 - \mu_p^2 \omega_x^2 Q_p^2\right] \ . \tag{5.7}$$

Thus the canonical momentum conjugate to $Q_p$ is $P_p \equiv \partial L / \partial \dot{Q}_p = M \dot{Q}_p$, and we can write the Hamiltonian as

$$H\left(p_m, q_m\right) = \frac{1}{2M} \sum_{p=1}^{N} P_p^2 + \frac{M}{2} \sum_{p=1}^{N} (\omega_x \mu_p)^2 Q_p^2 \ . \tag{5.8}$$

The quantum motion of the ions can now be considered by introducing the operators:

$$Q_p \rightarrow \hat{Q}_p \ = \ i \sqrt{\frac{\hbar}{2M\omega_x \mu_p}} \left(\hat{a}_p - \hat{a}_p^\dagger\right) \ , \tag{5.9}$$

$$P_p \rightarrow \hat{P}_p \ = \ \sqrt{\frac{\hbar M \omega_x \mu_p}{2}} \left(\hat{a}_p + \hat{a}_p^\dagger\right) \ . \tag{5.10}$$

where $\hat{Q}_p$ and $\hat{P}_p$ obey the canonical commutation relation $\left[\hat{Q}_p, \hat{P}_q\right] = i\hbar\delta_{pq}$ and the creation and annihilation operators $\hat{a}_p^\dagger$ and $\hat{a}_p$ obey the usual commutation relation $\left[\hat{a}_p, \hat{a}_q^\dagger\right] = \delta_{pq}$.

We shall use the interaction picture to perform calculations of the effect of laser fields on the trapped ions. The unperturbed Hamiltonian describes the free evolution of the internal states of the ions and the oscillations of the ions' normal modes. The effect of the laser field will be described by an interaction Hamiltonian introduced below. The interaction picture operator for the displacement of the m-th ion from its equilibrium position is:

$$\hat{q}_m(t) \ = \ \sum_{p=1}^{N} b_m^{(p)} \hat{Q}_p(t) \tag{5.11}$$

$$= \ i \sqrt{\frac{\hbar}{2M\omega_x N}} \sum_{p=1}^{N} s_m^{(p)} \left(\hat{a}_p e^{-i\omega_x \mu_p t} - \hat{a}_p^\dagger e^{i\omega_x \mu_p t}\right) \ , \tag{5.12}$$

where the coupling constant is defined by

$$s_m^{(p)} = b_m^{(p)} \sqrt{N/\mu_p} \ . \tag{5.13}$$

For the CM mode (p=1), which is the most important mode for quantum computation, $s_m^{(1)} = 1$ for all ions $m = 1, 2, \ldots N$.

## 5.2 Laser-ion interactions

### 5.2.1 "V" Type Operations: Single Qubit Interactions

There are two different ways of performing quantum computational laser operations on the qubits formed from two-level ions. The most simple is the single frequency Rabi oscillations between two states. If the two level system interacts with a monochromatic field precisely tuned to the transition frequency for the two levels, the population will oscillate back and forth between the two levels (fig. 3.a) [47, 48]. A long-lived two level system is required to make a qubit suitable for quantum computation, and so atomic levels with dipole-forbidden transitions are the most suitable. An example of such a dipole forbidden transition is the 729 nm $4\,^2S_{1/2}$ to $3\,^2D_{5/2}$ transition in $Ca^+$ (fig.2), which has a natural lifetime of about 1.06 seconds (see ref.[49] for more details and references to the sources of atomic data).

The other method of performing manipulations on the qubits of an ion trap quantum computer is to use Raman transitions (fig.3.b). This technique was used by the Boulder group in their experimental realization of a quantum logic gate using a cold trapped ion [10]. Two lasers, traditionally named the "pump" and the "Stokes" beams, are tuned so that population from one level is pumped to some intermediate virtual level by one laser, and then immediately brought back down from the virtual level to a different atomic state by the second laser [50, 51]. This method has some advantages over the single laser technique, because it is resilient against phase fluctuations of the addressing laser and because one can use two states with *very* long decay times, for example the two magnetic sub-levels of the $4\,^2S_{1/2}$ level of $Ca^+$. However it also has the complication that one needs to precisely control the position and direction of two laser beams rather than the one required for the first method. It may be that for the experimental devices now under construction, which will consist of only a few qubits, the first technique will prove superior.

The interaction picture Hamiltonian describing the resonant interaction of a two

level system with a laser can be written as follows:

$$\hat{H}_I = \frac{i\hbar\Omega_0}{2} \exp(i\Delta t)|0\rangle\langle 1| + h.a. \tag{5.14}$$

where $h.a.$ stands for the Hermitian adjoint of the immediately preceding term. The Rabi frequency $\Omega_0$ is defined by

$$\Omega_0 = \begin{cases} \frac{eE}{\hbar}\sqrt{\frac{A}{c\alpha k^3}}\beta & \text{(single laser)} \\ \\ \frac{e^2 A}{\hbar^2 c\alpha k^3}\frac{E_p E_s^*}{4\delta}\beta & \text{(Raman)} \end{cases} \tag{5.15}$$

In these formulas, $\beta$ is a coefficient of order 1 which depends on the laser polarizations and the quantum numbers of the states involved (for details see [49, 51]); $E$ is the complex electric field strength for the single laser; $E_p$ and $E_s$ are the complex electric field strengths of the pump and Stokes lasers respectively; $A$ and $k$ are, in the single laser case, the Einstein A coefficient and the wavenumber for the qubit transition, and in the Raman case, the A coefficient and the wavenumber for the transition from the two qubit levels $|0\rangle$ and $|1\rangle$ to the third detuned level, $|2\rangle$ (see fig.3) [4]; $\delta$ is the detuning of the virtual level from level $|2\rangle$. The detuning, $\Delta$, which appears in eq.(5.14) is given by the following formula:

$$\Delta = \begin{cases} \omega_0 - \omega_L & \text{single laser} \\ \\ \omega_0 - (\omega_p - \omega_s) & \text{Raman} \end{cases} \tag{5.16}$$

where $\omega_0$ is the angular transition frequency for the $|0\rangle$ to $|1\rangle$ transition, $\omega_L$ is the angular laser frequency (single laser case) and $\omega_p$ and $\omega_s$ are the pump and Stokes angular frequencies respectively (Raman case) [5].

If we assume that the detuning in eq.(5.14) is zero, and that only the states $|0\rangle$ and $|1\rangle$ can become populated, i.e. the wavefunction for the qubit is $|\psi(t)\rangle = a(t)|0\rangle + b(t)|1\rangle$, then the equation of motion,

$$i\hbar\frac{\partial}{\partial t}|\psi(t)\rangle = \hat{H}_I|\psi(t)\rangle, \tag{5.17}$$

[4] If $|0\rangle$ and $|1\rangle$ are magnetic sublevels of the same level, then the value of $A$ will be the same for them both.

[5] We have ignored the A.C. Stark shifts of the two qubit levels caused by the two Raman lasers. This effect will mean that the on-resonance condition will not be exactly $\Delta = 0$, and there will be a small phase shift in the execution of CNOT gates as a result. This is discussed in detail in ref.[51]

has the following solution:

$$\begin{pmatrix} a(t) \\ b(t) \end{pmatrix} = \begin{pmatrix} \cos(\theta/2) & ie^{i\phi}\sin(\theta/2) \\ ie^{-i\phi}\sin(\theta/2) & \cos(\theta/2) \end{pmatrix} \begin{pmatrix} a(0) \\ b(0) \end{pmatrix} \tag{5.18}$$

where $\theta = |\Omega_0|t$ and $\phi = \arg\{\Omega_0\}$.

Thus, by directing an on-resonance laser pulse at a particular ion, an arbitrary superposition of the $|0\rangle$ and $|1\rangle$ states can be created from the $|0\rangle$ state by carefully controlling the duration and phase of the pulse. The effect of such a pulse, which we will refer to as a "V" pulse, on the m-th ion's internal states is represented by the single-ion unitary operation, $\hat{V}_m(\theta, \phi)$,

$$\hat{V}_m(\theta,\phi): \begin{array}{lcl} |0\rangle_m & \rightarrow & \cos(\theta/2)|0\rangle_m - ie^{i\phi}\sin(\theta/2)|1\rangle_m \\ |1\rangle_m & \rightarrow & \cos(\theta/2)|1\rangle_m - ie^{-i\phi}\sin(\theta/2)|0\rangle_m \end{array}. \tag{5.19}$$

For example, $\theta = \pi$ is a $\pi$-pulse, which changes $|0\rangle$ into $|1\rangle$ and vice-versa (with a $\pi$ phase shift):

$$\hat{V}_m(\pi,\pi/2): \begin{array}{lcl} |0\rangle_m & \rightarrow & |1\rangle_m \\ |1\rangle_m & \rightarrow & -|0\rangle_m \end{array} \tag{5.20}$$

Similarly, the operation $\hat{V}(\pi/2, \pi/2)$, a $\pi/2$ pulse, creates equally-weighted superpositions of the basis states; A $2\pi$ pulse produces a sign change of the state in the same way that a rotation of $2\pi$ produces a sign change of the wavefunction of a spin-1/2 particle; a $4\pi$ pulse returns the ion to its original state.

However, these operations all have the form of a rotation, whereas quantum logical operations are required that have the form of a reflection, such as the NOT operation:

$$NOT: \begin{array}{lcl} |0\rangle_m & \rightarrow & |1\rangle_m \\ |1\rangle_m & \rightarrow & |0\rangle_m \end{array} \tag{5.21}$$

and the single-bit Hadamard operation:

$$\hat{R}: \begin{array}{lcl} |0\rangle_m & \rightarrow & (|0\rangle_m + |1\rangle_m)/\sqrt{2} \\ |1\rangle_m & \rightarrow & (|0\rangle_m - |1\rangle_m)/\sqrt{2}. \end{array} \tag{5.22}$$

We can perform these operations with the aid of an *auxiliary level*, $|aux\rangle$. The auxiliary level, which is a vital ingredient of Cirac and Zoller's scheme, is some third state of the ion which will interact with $|0\rangle$ in precisely the same manner as $|0\rangle$ interacts with $|1\rangle$, but which does not interact at all with $|1\rangle$. For example, we can use the $4^2S_{1/2}$, $M_J = 1/2$ and the $3^2D_{5/2}$, $M_J = 3/2$ states of $Ca^+$ as $|0\rangle$ and $|1\rangle$ for our qubits. The auxiliary level can then be the $3^2D_{5/2}$, $M_J = -1/2$ state. We can perform operations between $|0\rangle$ and $|1\rangle$ using right-hand circularly polarized light. If we switch

to left circularly polarized light we can perform operations between $|0\rangle$ and $|aux\rangle$, without changing the state of $|1\rangle$. The unitary operations involving $|0\rangle$ and $|aux\rangle$ will be denoted as follows:

$$\hat{V}_m^{(aux)}(\theta,\phi): \begin{array}{lcl} |0\rangle_m & \rightarrow & \cos(\theta/2)\,|0\rangle_m - ie^{i\phi}\sin(\theta/2)\,|aux\rangle_m \\ |aux\rangle_m & \rightarrow & \cos(\theta/2)\,|aux\rangle_m - ie^{-i\phi}\sin(\theta/2)\,|0\rangle_m \end{array} \tag{5.23}$$

Using this operation $\hat{V}_m^{(aux)}$ in conjunction with $\hat{V}_m$ , we can perform the NOT and single bit Hadamard transforms on the m-th qubit as follows:

$$NOT_m = \hat{V}_m^{(aux)}(2\pi,\pi/2)\,\hat{V}_m(\pi/2,\pi/2) \tag{5.24}$$

$$\hat{R}_m = \hat{V}_m^{(aux)}(2\pi,\pi/2)\,\hat{V}_m(3\pi/2,\pi/2)\,. \tag{5.25}$$

### 5.2.2 "U" Type Operations: Interactions with the Quantum Bus Channel

To describe the ability of the laser beam to excite or annihilate quanta of the ions' collective vibrations, it is necessary to modify the interaction Hamiltonian (5.14) by taking into account the spatial variation of the the laser field as follows:

$$\begin{aligned} E \rightarrow E(\hat{\mathbf{r}}_m) &= E(\mathbf{r}_m^0 + \mathbf{e}_x\hat{q}_m) \\ &\approx E_{eq} + \hat{q}_m\left(\frac{\partial E}{\partial x}\right)_0 \end{aligned} \tag{5.26}$$

where $\mathbf{r}_m^0$ is the equilibrium position of the m-th ion, $\mathbf{e}_x$ is the unit vector in the axial (x) direction, $\hat{q}_m$ is the quantum operator describing the vibration of the m-th ion (see 5.12) and the subscript 0 denotes a term which has been evaluated at the equilibrium position of the ion. For simplicity, we shall neglect all of the phonon modes except for the CM mode (p=1). We therefore obtain the following modified form of the interaction Hamiltonian:

$$\begin{aligned} \hat{H}_I &= \frac{i\hbar\Omega_0}{2}\exp(i\Delta t)|0\rangle\langle 1| \\ &+ \frac{i\hbar\Omega_1}{2}\exp(i\Delta t)|0\rangle\langle 1|\left[\hat{a}\exp(-i\omega_x t) - \hat{a}^\dagger\exp(i\omega_x t)\right] + h.a. \end{aligned} \tag{5.27}$$

Here $\Omega_0$ is given by eq.(5.15), and

$$\Omega_1 = \sqrt{\frac{\hbar}{2M\omega_x N}}\left(\frac{\partial\Omega_0}{\partial x}\right)_{eq}, \tag{5.28}$$

where the partial derivative acts only on the spatial variations of the electric fields. For plane waves, which will be a good approximation for the focal regions of Gaussian

laser beams in the vicinity of an ion, $\Omega_1$ is given by the formula

$$\Omega_1 = \frac{\eta}{\sqrt{N}}\Omega_0, \tag{5.29}$$

where $\eta$ is the Lamb-Dicke parameter defined by:

$$\eta = \begin{cases} \sqrt{\frac{\hbar}{2M\omega_x}}\mathbf{k}_L \cdot \mathbf{e}_x & \text{(single laser)} \\ \sqrt{\frac{\hbar}{2M\omega_x}}(\mathbf{k}_p - \mathbf{k}_s) \cdot \mathbf{e}_x & \text{(Raman)} \end{cases} \tag{5.30}$$

$\mathbf{k}_L$, $\mathbf{k}_p$ and $\mathbf{k}_s$ being, respectively the wavevectors of the single laser, the pump laser and the Stokes laser. [6]

In order to realize quantum logic gates of the type devised by Cirac and Zoller, one sets the detuning, $\Delta = -\omega_x$. In this case, ignoring the off-resonant terms, eq. (5.27) becomes

$$\hat{H}_I = \frac{-i\hbar\Omega_1}{2}\hat{a}^\dagger|0\rangle\langle 1| + h.a. \tag{5.31}$$

This Hamiltonian is equivalent to that introduced by Jaynes and Cummings to describe the interaction of a two-level system with a single quantized harmonic oscillator [53]. If we assume that we are limited to two possible states: $|1\rangle \otimes |0 \text{ phonons}\rangle$ and $|0\rangle \otimes |1 \text{ phonon}\rangle$, which we shall denote as $|1,0\rangle$ and $|0,1\rangle$ respectively, the wavefunction for the ion is $|\psi'(t)\rangle = c(t)|0,1\rangle + d(t)|1,0\rangle$. The equation of motion (5.17) can then be solved:

$$\begin{pmatrix} c(t) \\ d(t) \end{pmatrix} = \begin{pmatrix} \cos(\theta'/2) & ie^{i\phi'}\sin(\theta'/2) \\ ie^{-i\phi'}\sin(\theta'/2) & \cos(\theta'/2) \end{pmatrix} \begin{pmatrix} c(0) \\ d(0) \end{pmatrix} \tag{5.32}$$

where $\theta' = |\Omega_1|t$ and $\phi' = \arg\{\Omega_1\}$. Thus we have interactions which change the CM phonon vibrational mode as well as the ions' internal levels in a controllable manner. We shall refer to such laser interactions as "U" type pulses. The following operation can be realized by these interactions with precise control of the pulse duration and laser phase:

$$\hat{U}_m(\theta', \phi'): \begin{array}{rcl} |0,1\rangle_m & \rightarrow & \cos(\theta'/2)\,|0,1\rangle_m - ie^{i\phi'}\sin(\theta'/2)\,|1,0\rangle_m \\ |1,0\rangle_m & \rightarrow & \cos(\theta'/2)\,|1,0\rangle_m - ie^{-i\phi'}\sin(\theta'/2)\,|0,1\rangle_m \end{array} \tag{5.33}$$

A similar transform $\hat{U}_m^{aux}$ can be defined between the $|0,1\rangle$ state and the $|aux,0\rangle$ state. It is important to emphasize that, because the phonon modes are *collective* oscillations,

[6] The expression (5.15) is an approximation which is valid if $\eta/\sqrt{N} \ll 1$. In general the expression for $\Omega_0$ depends on the number of phonons in the system; Monroe *et al.* recently pointed out that this fact allows one, in principal, to realize quantum gates more simply than by using the Cirac and Zoller auxiliary level scheme [52].

when the m-th ion acquires an amplitude in the $|1\text{ phonon}\rangle$ state, then all of the other ions in the trap also acquire an amplitude in the $|1\text{ phonon}\rangle$ state. This amplitude is dependent on the state of the m-th ion. Thus by means of interaction with the CM phonon mode, the internal state of any ion in the trap can be changed conditionally on the internal state of any other ion. The two-level system $\{|0\text{ phonons}\rangle, |1\text{ phonon}\rangle\}$ can be considered as an additional qubit that acts as a quantum bus channel, that can be used to transfer quantum information between different ions in the quantum register.

From these basic building blocks, a CNOT gate between ions c ("control") and t ("target") can be constructed from the sequence of five laser pulses

$$CNOT_{ct} = \hat{V}_t(\pi/2, \pi/2)\hat{U}_c\,(\pi, 0)\,\hat{U}_t^{aux}\,(2\pi, 0)\,\hat{U}_c\,(\pi, 0)\,\hat{V}_t(\pi/2, \pi/2). \tag{5.34}$$

## 5.3 Readout

Once the computational state manipulations required are completed, the result must be read out, which means that the state of each qubit must be measured. This can be accomplished using the quantum jump technique, which is relatively straightforward when using the single laser qubit scheme. For example, with $Ca^+$ ions, each qubit consists of a sub-level of the $4\,^2S_{1/2}$ ground state, $|0\rangle$, and a sub-level of the $3\,^2D_{5/2}$ metastable excited state, $|1\rangle$, (see fig.2). This qubit can be interrogated with the laser tuned to the $4\,^2S_{1/2}$ to $4\,^2P_{1/2}$ dipole transition at 397nm. If the ion radiates, its state has been collapsed to the $|0\rangle$ state, whereas if it remains dark then its state has collapsed to the $|1\rangle$ state. The $4\,^2P_{1/2}$ level can also decay to the $3\,^2D_{3/2}$ level, and so a pump-out laser at 866nm will also be required in order to stop population being trapped in that metastable level.

With the Raman scheme, readout is a little more complicated. Assume that $|0\rangle$ and $|1\rangle$ are the $M_J = -1/2$ and $M_J = +1/2$ sublevels of the $4\,^2S_{1/2}$ ground state, respectively. The most straightforward method of performing the readout in these circumstances is to apply a $\pi$ pulse from the $|1\rangle$ (or $|0\rangle$) state to a sub-level of the $3\,^2D_{5/2}$ state, and then use a laser at 397nm to observe fluorescence (if any) due to population in the $|0\rangle$ (or $|1\rangle$) state, as in the single laser scheme. Alternatively, a $\sigma^-$ circularly polarized laser at 393nm can excite population from $|0\rangle$ state to the $M_J = -3/2$ sub-level of the $4\,^2P_{3/2}$ level, which will decay by dipole emission back to $|0\rangle$. One can avoid exciting population from the $|1\rangle$ level by applying a sufficiently strong magnetic field that the transition from this state to the $4\,^2P_{3/2}\,M_J = -1/2$

sub-level is shifted off resonance by the Zeeman effect (a magnetic field of 200 Gauss should be sufficient for this purpose). However, the $4\,^2P_{3/2}M_J = -3/2$ sub-level can also decay to both the $3\,^2D_{3/2}$ and $3\,^2D_{5/2}$ levels, and pumping out the population trapped in these states might be lead to difficulties.

## 5.4 Tolerances and Laser Requirements

### 5.4.1 Pulse Durations and Standing Waves

In deriving the formulas that describe the effects of laser pulses on the qubits we have made various assumptions which allow us to discard off-resonant terms in the Hamiltonian. The criteria for making these approximations place constraints on the experimental parameters, in particular the duration of the various laser pulses required to perform operations.

For the V-type pulses, we have neglected terms involving coupling to phonon modes. These can be neglected provided that $(\Omega_1/\omega_x)^2 \ll 1$. Using eq. 5.28, and the fact that the duration of a V-type $\pi$ pulse is $t_V = \pi/\Omega_0$, we find that the pulse duration must obey the following inequality:

$$t_V \gg \frac{\pi\eta}{\sqrt{N}\omega_x}. \tag{5.35}$$

For 10 $Ca^+$ ions in a trap with a $2\pi \times 500$ kHz axial angular frequency, eq.(5.35) implies that $t_V \gg 7.5$ nsec for the single laser scheme and $t_V \gg 14$ nsec for the Raman scheme. This condition will become easier to satisfy as the number of ions $N$ grows large.

For U-type pulses, we have neglected the terms in the interaction Hamiltonian (5.27) which give rise to "direct" transitions, i.e. those that do not involve the creation or annihilation of a phonon. Using a similar argument, one can show that the duration of a U-type $\pi$-pulse must obey the following inequality:

$$t_U \gg \frac{\pi\sqrt{N}}{\eta\omega_x} \text{ (traveling wave).} \tag{5.36}$$

Thus if we have a large number of ions in our trap, the duration of the sideband detuned U pulses must become very long. Using the same example that we quoted for the V pulses, i.e. 10 $Ca^+$ ions in a $2\pi \times 500$ kHz trap, (5.36) implies that $t_U \gg 130\,\mu$sec for the single laser scheme and $t_U \gg 72\,\mu$sec for the Raman scheme.

A method by which these pulse durations can be made shorter has been suggested by Cirac and Zoller and co-workers ([9, 54]). If one were to apply the laser field in a configuration such that $\Omega_0$ were zero, but $\Omega_1$ was non-zero, then the direct transition

terms in the Hamiltonian (5.27) would be zero. For example, the single laser could be used in a standing wave configuration such that one has a node at the location of the ion one is trying to address [7] . In these circumstances, one would still have to worry about the possibility of exciting the "wrong" phonon modes, and it can be shown [49] that this places the following constraint on the duration of U-type $\pi$ pulses:

$$t_U \gg \frac{2.6\pi}{\omega_x} \text{ (standing wave).} \tag{5.37}$$

This has the advantage that the duration of U-type pulses is independent of the number of ions in the trap. Again using the example of 10 $Ca^+$ ions in a $2\pi \times 500$ kHz trap, the durations of the U-pulses must be $t_U \gg 2.6\,\mu$sec when we have standing waves. However there are considerable technical difficulties in arranging a laser beam, which must have a component of its wavevector parallel to the trap axis, in a standing wave configuration, with all of the ions either at a node or an anti-node. Thus for the small number of ions which will be involved in the first generation ion-trap quantum computers, it seems that the practical problems associated with building an optical system that allows us to address the ions with standing waves will outweigh the advantages of having shorter pulses. However, they will probably be *required* if we are to have a computer with more than a few qubits.

### 5.4.2 Laser Power Requirements

The expressions for the Rabi frequencies, eqs.(5.15) and (5.28), relate the rate of flipping between the two levels $|0\rangle$ and $|1\rangle$ to the electric field strength of the lasers. From these formulas, we can derive an expression relating the laser power to the duration of the various pulses. This is important information to know when determining the specifications of the laser system which must be built. The power in a Gaussian laser beam is given by (ref. [55], eq.14.5.27, p.488)

$$P = \frac{c\epsilon_0}{4}\pi w_0^2 |E|^2, \tag{5.38}$$

where $c$ is the velocity of light, $\epsilon_0$ is the permittivity of the vacuum and $w_0$ is the $1/e^2$ radius of the focal spot. On substituting from eq. (5.28), we find the laser power is

[7] Note that the roles of nodes and anti-nodes are reversed for quadrupole allowed transitions. For details, see ref.[49].

given by the following expression:

$$P \approx \begin{cases} \dfrac{\hbar w_0^2 \omega_L \omega_x NM}{A t_U^2} & \text{(single laser)} \\ \\ \dfrac{\hbar w_0^2 \omega_L^2 \delta NM}{cAt_U} \sqrt{NM\hbar\omega_x} & \text{(Raman)} \end{cases} . \tag{5.39}$$

We have assumed that, in the Raman case, the pump and Stokes lasers have approximately the same power. In these formulas, $t_U$ is the duration of a U-type $\pi$-pulse, i.e. $t_U = \pi/\Omega_1$; the other symbols have the same meaning as given above (see the paragraph following eq.(5.15)). For 10 Calcium ions, assuming a pulse duration $t_U$ of 5 $\mu$sec (which is compatible with the minimum pulse duration when standing waves are employed), a laser spot size $w_0$ of 10 $\mu$m, an axial frequency $\omega_x$ of $2\pi\times500$ kHz, and a Raman detuning $\delta$ of $2\pi\times100$ MHz, the power required for the single laser scheme is 25 mW, compared to a required power of 0.11 $\mu$W for the Raman scheme. Longer pulses, which would be required if standing waves are not used, would need *less* power.

### 5.4.3 Error Rates and Fault Tolerant Quantum Computing

In the two years since Cirac and Zoller's original proposal was published, there have been several calculations of the limitations of the capabilities of such devices due to various decoherence effects [23, 24, 25]. While these investigations are useful for identifying theoretically the various important decoherence processes, none of them take into account the recent breakthroughs in the realm of fault tolerant quantum computation [11, 12]. As mentioned in the introduction, it has been demonstrated that, provided quantum gates can be performed within a certain threshold degree of accuracy (the most optimistic estimate of which is $\sim 10^{-6}$), then in principle arbitrarily large quantum computations can be performed accurately. This sets an obvious figure of merit for quantum computation technology, namely, the expected probability of error in one quantum gate.

For trapped ion quantum computers using the single laser addressing scheme, there are two principal fundamental causes of error which we must examine: spontaneous emission from the upper level of the qubit, and breakdown of the two-level system. The first suggests that we should use the *shortest* possible laser pulses, so that the gate operation is completed quickly, before the upper level can decay. The second type of error is reduced by using very low laser powers, and so *long* duration laser pulses should be the best. Thus there is an optimum situation when these two effects balance. If

we then use the limiting cases given by eqs.(5.36) and (5.37), we obtain the following expression for the minimum possible error probability per CNOT using $Ca^+$ ions:

$$\varepsilon \sim \begin{cases} 8.9 \times 10^{-6} N^{1/3} & \text{(standing wave)} \\ 3.6 \times 10^{-5} N^{1/2} & \text{(traveling wave)} \end{cases} \tag{5.40}$$

Thus although the use of standing waves will reduce the error significantly, it still does not appear that it will be possible to meet the existing accuracy thresholds using single laser addressing. (Other species of ion give similar results.) This, however, does not imply that quantum computation experiments using single laser addressing are without merit; discounting the possibility that further theoretical advances may reduce the error threshold, the single laser system will still be useful as a experimental device for performing limited gate operations on a dozen or so qubits, which will allow one to confirm both the practicality of quantum computation with cold trapped ions, as well as aspects of the theory of fault tolerant quantum computation.

Using the Raman system, the fundamental source of error we have to worry about is spontaneous emission from the upper level $|2\rangle$ of the three level system (see fig. 3.b). As the average population in this level and the rate at which the quantum gate is performed are both proportional to the laser power, the error rate can be shown to be *independent* of the duration of the laser pulses [71]. One can minimize this error by using the largest possible Raman detuning $\delta$ and the smallest possible axial frequency $\omega_x$. However, when one is detuned from one level by a large amount, one can come into resonance with another level; hence, when calculating the error, *all* of the ion's levels must be taken into account. The smallest practical trap frequency can be estimated to be 100 Hz, although the experimental problems associated with cooling at this frequency are more than a little daunting. In this case, the error per gate for $Ca^+$ ions is

$$\varepsilon \sim 1.3 \times 10^{-8} N^{1/2}. \tag{5.41}$$

This implies that in theory it may be possible to perform reliable quantum computations, with errors per gate of the order of $10^{-6}$, with $\sim$100 $Ca^+$ ions. Similar calculations give even larger numbers ($\sim$5000) for $Be^+$ ions. The estimates should be viewed with a great deal of caution: throughout the work done on fault tolerant techniques, the assumption was made that the error rate per gate was independent of the number of qubits, and so large numbers of qubits could be used without undue penalty. When the error rate is dependent on the number of qubits, as is the case here, the results are no longer valid. However, they do suggest that some optimism regarding the future of ion trap quantum computation may not be unwarranted.

# 6 Experimental Considerations

## 6.1 Choice of Ion

There are three requirements which the species of ion chosen for the qubits of an ion trap quantum computer must satisfy:

1. If we use the single laser scheme, the ions must have a level that is sufficiently long-lived to allow some computation to take place; this level can also be used for sideband cooling.

2. the ions must have a suitable dipole-allowed transition for Doppler cooling, quantum jump readout and for Raman transitions (if we chose to use two sub-levels of the ground state to form the qubit);

3. These transitions must be at wavelengths compatible with current laser technology.

Various ions used in atomic frequency standards work satisfy requirement 1: A long-lived transition will have a very narrow spectral line which can be exploited for that application. Examples are $Hg^+$, $Ca^+$ or $Ba^+$ (which have quadrupole allowed transitions in the optical, near infrared or near ultraviolet regions of the spectrum, with lifetimes ranging from hundreds of milliseconds to several seconds; for details, see [49]). An even more exotic possibility is $Yb^+$ which has an optical electric octupole transition with a lifetime of about 10 years [56]. Of these ions, $Ca^+$ offers the advantages of transitions that can be accessed with titanium-sapphire or diode lasers and a reasonably long-lived metastable state. The relevant energy levels of the $A = 40$ isotope are shown in fig.2. The dipole-allowed transition from the $4\,^2S_{1/2}$ ground state to the $4\,^2P_{1/2}$ level with a wavelength of 397 nm can be used for Doppler cooling and quantum jump readout; The 732 nm electric quadrupole transition from the $4\,^2S_{1/2}$ ground state to the $3\,^2D_{3/2}$ metastable level (lifetime $\approx 1.08sec.$) is suitable for sideband cooling. In the single laser computation scheme, the qubits and auxiliary level can be chosen as the electronic states

$$|0\rangle = |4\,^2S_{1/2},\, M_j = 1/2\rangle,\ |1\rangle = |3\,^2D_{5/2},\, M_j = 3/2\rangle,\ |aux\rangle = |3\,^2D_{5/2},\, M_j = -1/2\rangle \tag{6.1}$$

The $\hat{V}$ and $\hat{U}$ operations can be driven using left-handed circular polarized 729-nm radiation, while the $\hat{V}^{aux}$ and $\hat{U}^{aux}$ operations require right-handed circular polarization.

This ion can also be used for Raman type qubits, with the two Zeeman sublevels of the $4\,^2S_{1/2}$ ground state forming the two qubit states $|0\rangle$ and $|1\rangle$, with one of the

sublevels of the $4\,^2P_{1/2}$ level being the upper level $|2\rangle$. As mentioned above, a magnetic field of 200 Gauss should be sufficient to split these two levels so that they can be resolved by the lasers. The pump and Stokes beams would be formed by splitting a 397nm laser into two, and shifting the frequency of one with respect to the other by means of an acousto-optic or electro-optic modulator. This arrangement has a great advantage in that any fluctuations in the phase of the original 397nm laser will be passed on to both the pump and Stokes beams, and will therefore be canceled out, because the dynamics is only sensitive to the difference between the pump and Stokes phases. One problem in realizing the Raman scheme in $Ca^+$ is the absence of a third level in the ground state that can act as the auxiliary state $|aux\rangle$ required for execution of quantum gates. This difficulty could be removed by using the alternative scheme for quantum logic recently proposed by Monroe *et al.* [52]; alternatively, one could use an isotope of $Ca^+$ which has non-zero nuclear spin, thereby giving several more sublevels in the ground state due to the hyperfine interaction [8]; other possibilities that have been suggested for an auxiliary state with $^{40}Ca^+$ in the Raman scheme are to use a state of a phonon mode other than the CM mode [58] or one of the sublevels of the $3\,^2D$ doublet [59].

## 6.2 The Radio Frequency Ion Trap

Radio-frequency (RF) quadrupole traps, also named "Paul traps" after their inventor, have been used for many years to confine electrically charged particles [60] (for an introduction to the theory of ion traps, see refs. [61, 62]). The classic design of such a Paul trap has a ring electrode with endcap electrodes above and below, with the ions confined to the enclosed volume. A single ion can be located precisely at the center of the trap where the amplitude of the RF field is zero. But when several ions are placed into this trapping field, their Coulomb repulsion forces them apart and into regions where they are subjected to heating by the RF field. For this reason in our experiment ions are confined in a linear RF quadrupole trap. Radial confinement is achieved by a quadrupole RF field provided by four 1 mm diameter rods in a rectangular arrangement. Axial confinement is provided by DC voltages applied to conical endcaps at either end of the RF structure; the endcap separation is 10 mm. The design of the trap used in these experiments is shown in diagrammatically in Figs.4 and 5. An image of a trapped ion is shown in Fig.6.

[8] The only such stable isotope of Calcium is $^{43}Ca$, which has nuclear spin 7/2 and a natural abundance of 0.135%. Enriched samples are available at a cost of $441 per mg [57].

The main concerns for the design are to provide sufficient radial confinement to assure that the ions form a string on the trap axis after Doppler cooling; to minimize the coupling between the radial and axial degrees of freedom by producing radial oscillation frequencies significantly greater than the axial oscillation frequencies; to produce high enough axial frequencies to allow the use of sideband cooling[63]; and to provide sufficient spatial separation to allow individual ions to be addressed with laser beams.

### 6.2.1 Radial Confinement

A sinusoidal voltage with a DC offset, $\Phi = \Phi_{DC} - \Phi_{RF}\cos(\omega_{RF}t)$, is applied to two opposite rods of the RF structure while the other two are grounded. The potential near the center of the trap is

$$\Phi = \Phi_o \frac{z^2 - y^2}{2r_o^2}, \tag{6.2}$$

where $r_o$ is a constant dependent on the distance from the trap axis to the RF rods and $y$ and $z$ are the distances from the trap axis along the y and z axes, respectively (see fig.1). For this trap, $r_o$ =1.4mm.

The equation of motion for an ion in this time-dependent quadrupole potential is the well known Matthieu's equation, the solutions of which [64] are parameterized in this case, by the quantities $a = 4e\Phi_{DC}/(M\omega_{RF}^2 r_o^2)$ and $q = 2e\Phi_{RF}/(M\omega_{RF}^2 r_o^2)$. For a proper choice of these parameters, the motion of the ion can be treated by a pseudopotential approach. Here, the ions are described as moving in the effective quadratic potential

$$\Phi^{(eff)} = \frac{e\Phi_{RF}^2 \rho^2}{4M\omega_{RF}^2 r_o^4}, \tag{6.3}$$

where $\rho = \sqrt{y^2 + z^2}$ is the radial distance from the trap axis. The total motion consists of a fast ripple superimposed on a slower, larger amplitude oscillation, referred to as the secular motion, of frequency

$$\omega_r = \frac{e\Phi_{RF}}{\sqrt{2}M\omega_{RF}r_o^2}. \tag{6.4}$$

Typical operating parameters for the trap described are $\Phi_{DC} = 0$, $\Phi_{RF} = 500$ Volts, and $\omega_{RF} = (2\pi)\times$ 11.5 MHz. This yields a radial pseudowell of 15 eV depth and a secular motion frequency of $\omega_r = (2\pi)\times$ 5 MHz. Laser cooling of the ions to the Doppler limit imposed by the natural linewidth of the $4\,^2S_{1/2} - 4\,^2P_{1/2}$ cooling transition will yield a temperature $T_{Dop} \approx 85\ \mu$K. Comparing this thermal energy with

the radial pseudowell depth, we find that the ions should be confined to within roughly 30 nm of the trap axis after Doppler cooling.

### 6.2.2 Axial Confinement

As mentioned above, axial confinement is provided by conical electrodes at either end of the RF structure. The conical shape allows maximum laser access while providing a large region at the trap center for which the potential is harmonic. A static bias voltage of up to 500 V is applied to both endcaps.

When the ions are sufficiently cold, they will crystallize to form a line or "string of pearls". In this configuration the axial force on the m-th ion due to the harmonic binding potential and the Coulomb force upon it due to all of the other ions is given by the formula

$$F_m = M\omega_x^2 x_m + \sum_{\substack{n=1 \\ m\neq n}}^{N} \frac{e^2}{4\pi\epsilon_0} \frac{1}{(x_n - x_m)^2} \ , \tag{6.5}$$

where the symbols have the same meaning as in eq.(5.3). The equilibrium positions of the ions are determined by the set of $N$ equations, $F_m = 0$, $(m = 1, 2, \ldots N)$. For $N = 2$ or $N = 3$, the equations may be solved analytically; for larger values of $N$ numerical solutions must be found. For details, see ref. [49]. We find that the minimum inter-ion spacing (which will occur at the middle of the string) for $N$ ions and axial frequency $\omega_x$ is given by:

$$x_{min}(L) = \left( \frac{e^2}{4\pi\epsilon_0 M\omega_x^2} \right)^{1/3} \frac{2.018}{N^{0.559}} \ . \tag{6.6}$$

This relationship is important in determining the extent of "cross-talk" error in a quantum computer, due to the focal region of lasers overlapping more than one ion. [23]. Figure 7 shows this calculated minimum equilibrium separation as a function of axial oscillation frequency, which is proportional to the square root of the applied trapping voltage. The curve is truncated at $(2\pi)\times$500 kHz, because, as discussed earlier we are interested only in frequencies significantly lower than the 5 MHz secular frequency. Preliminary numerical model calculations [65] for our trap geometry indicated that an endcap voltage of 150 V would yield an axial trapping frequency of roughly $(2\pi)\times$200 kHz. We have experimentally verified this prediction by observing resonance ion heating through parametric excitation of the axial oscillation of the ions. Small number of ions were trapped and laser cooled. A weak RF drive was coupled to the DC input

applied to the end caps. The frequency was slowly varied and when the applied frequency was equal to $2 \times \omega_x$ a strong heating of the ion cloud was observed. Figure 8 shows the results of these tests in comparison to the numerical calculations. The solid line is a fit to the data assuming a strict quadratic relation between axial frequency and trap potential. The proportionality constant gives the shielding of the external potential by the trap electrodes. As can be seen, when there are two ions in the trap a frequency of $(2\pi)\times$200 kHz corresponds to an ion separation of approximately 20 $\mu$m. Hence, to resolve the axial motion sidebands on the ion fluorescence signal and to cool the ions to the vibrational ground level of the axial well, laser linewidths well under $(2\pi)\times$200 kHz will be required. Furthermore, gate operations involving manipulations of individual ions will require laser spot sizes well under 20 $\mu$m.

The linear configuration of the ions will break down if there are too many ions in the trap. The Coulomb force from ions at the ends of the string will become so great that the radial confinement will become unstable, and the ions will adopt a zig-zag configuration, which is susceptible to RF heating. The radial confinement is characterized by a harmonic frequency $\omega_r$, given by eq. (6.4). Numerical modeling of the zig-zag breakdown (based on the instability of the transverse oscillation modes) gives the following formula for the maximum number of ions that can reside in a linear configuration:

$$N_{max} = 1.82 \left( \frac{\omega_r}{\omega_x} \right)^{1.13}. \tag{6.7}$$

This formula is in general agreement with that previously worked out by numerical modeling of cold confined plasmas [27]. In the ion trap used in our experiment, $\omega_r = 2\pi \times 5$MHz and $\omega_x$ can be in the range from $2\pi \times 500$kHz to $2\pi \times 100$kHz. Thus the largest number of ions that can be stored in this specific system in a linear configuration varies between 24 and 151 ions respectively.

### 6.2.3 Thermalization of Trapped Ions and Noise Driven Decoherence

We have theoretically investigated the effects of external noise sources (as opposed to trap RF effects) in regard to ion heating and decoherence [66]. Of the sources considered, which included mechanical vibrations, black body radiation, and Johnson noise, only the latter was found to be significant. By use of a result based on a classical model of the trapped ion [67], Wineland *et al.* [68] concluded that Johnson noise cannot account for the observed ion heating rate. We have carried the calculation further and have now shown that the heating rate (which in the case of Johnson noise is roughly

equal to the harmonic oscillator superposition state decoherence rate) can be explained within a reasonable range of system parameters.

The heating rate is proportional to the effective resistances connected across the trap electrodes. However, the fact that this resistance depends on the frequency of the noise fluctuations was not taken into account in [68] where it was concluded that the observed heating rate in a particular experiment was roughly 10 to 100 times faster than predicted by the use of the model in [67]. Our primary conclusions are that it is incorrect to use the DC resistance of the trap electrode interconnections to determine the heating rate, and that in many instances, better insight can be obtained through consideration of the noise correlation time. We hope to experimentally investigate the implications of our theoretical work in the near future.

## 6.3 Laser Systems

The relevant optical transitions for $Ca^+$ ions are shown in fig.2. There are four different optical processes employed in the quantum computer; each places specific demands on the laser system.

The first stage is to cool a small number of ions to their Doppler limit in the ion trap, as shown in fig.(9.a). This requires a beam at 397 nm, the $4\,^2S_{1/2} - 4\,^2P_{1/2}$ resonant transition. Tuning the laser to the red of the transition causes the ions to be slowed by the optical molasses technique [69]. In this procedure, a laser beam with a frequency slightly less than that of the resonant transition of an ion is used to reduce its kinetic energy. Owing to the Doppler shift of the photon frequency, ions preferentially absorb photons that oppose their motion, whereas they re-emit photons in all directions, resulting in a net reduction in momentum along the direction of the laser beam. Having carefully selected the trap parameters, many cycles of absorption and re-emission will bring the system to the Lamb-Dicke regime, leaving the ions in a string-of-pearls geometry.

In order to Doppler cool the ions, the demands on the power and linewidth of the 397 nm laser are modest. The saturation intensity of $Ca^+$ ions is $\sim 10$ mW/cm$^2$, and the laser linewidth must be less than $\sim 10$ MHz. An optogalvonic signal obtained with a hollow cathode lamp suffices to set the frequency. We use a Titanium:Sapphire (Ti:Sapphire) laser (Coherent CR 899-21) with an internal frequency doubling crystal to produce the 397 nm light.

During the Doppler cooling, the ions may decay from the $4\,^2P_{1/2}$ state to the $3\,^2D_{3/2}$ state, whose lifetime is $\sim$ 1sec. To empty this metastable state, we use a

second Ti:Sapphire laser at 866 nm.

Once the string of ions is Doppler cooled to the Lamb-Dicke regime, the second stage of optical cooling, sideband cooling, will be used to reduce the collective motion of the string of ions to its lowest vibrational level [70], illustrated in fig. (9.b). In this regime, a narrow optical transition, such as the 732 nm $4\,^2S_{1/2} - 3\,^2D_{3/2}$ dipole forbidden transition, develops sidebands above and below the central frequency by the vibrational frequencies of the ions. The sidebands closest to the unperturbed frequency correspond to the CM vibrational motion. If $\omega_0$ is the optical transition frequency and $\omega_x$ the frequency of the CM vibrational motion, the phonon number is increased by one, unchanged, or decreased by one if an ion absorbs a photon of frequency $\omega_0 + \omega_x$, $\omega_0$ or $\omega_0 - \omega_x$, respectively. Thus, sideband cooling is accomplished by optically cooling the string of ions with a laser tuned to $\omega_0 - \omega_x$.

The need to resolve the sidebands of the transition implies a much more stringent requirement for the laser linewidth; it must be well below the CM mode vibrational frequency of $\sim (2\pi) \times 200$ kHz. The laser power must also be greater in order to pump the forbidden transition. We plan to use a Ti:Sapphire laser locked to a reference cavity to meet the required linewidth and power. At first glance it would seem that, with a metastable level with a lifetime of 1s, no more than 1 phonon per second could be removed from a trapped ion. A second laser at 866 nm is used to couple the $4\,^2P_{1/2}$ state to the $3\,^2D_{3/2}$ state to reduce the effective lifetime of the D state and allow faster cooling times. The transitions required for realization of quantum logic gates and for readout, discussed in detail in sections 5.2 and 5.3, are shown in fig.(9.c). These can be performed with the same lasers used in the Doppler and sideband cooling procedures.

There are two other considerations concerning the laser systems for quantum computation which should be mentioned. To reduce the total complexity of the completed system, we are developing diode lasers and a frequency doubling cavity to handle the Doppler cooling and quantum jump read out. Also complex quantum computations would require that the laser on the $4\,^2S_{1/2} - 3\,^2P_{5/2}$ computation transition have a coherence time as long as the computation time. This may necessitate using qubits bridged by Raman transitions as discussed above, which eliminates the errors caused by the phase drift of the laser.

## 6.4 Qubit Addressing Optics

In order for the $Ca^+$ ion qubits to be useful for actual calculations, it will be necessary to address the ions in a very controlled fashion. Our optical system for qubit addressing

is shown schematically in fig. 10. There are two aspects to be considered in the design of such a system: the precise interactions with a single ion; and an arrangement for switching between different ions in the string. In addition to the obvious constraints on laser frequency and polarization, the primary consideration for making exact $\pi$- or $2\pi$-pulses is control of the area (over time) of the driving light field pulse. The first step toward this is to stabilize the intensity of the laser, as can be done to better than 0.1%, using a standard "noise-eater". Such a device typically consists of an electro-optical polarization rotator located between two polarizers; the output of a fast detector monitoring part of the transmitted beam is used in a feedback circuit to adjust the degree of polarization rotation, and thus the intensity of the transmitted light. Switching the light beam on and off can be performed with a similar (or even the same) device. Because such switches can possess rise/fall times on the scale of nanoseconds, it should be possible to readily control the area under the pulse to within $\sim 0.1\%$, simply by accurately determining the width of the pulse. A more elaborate scheme would involve an integrating detector, which would monitor the actual integrated energy under the pulse, shutting the pulse off when the desired value is obtained.

Once the controls for addressing a single ion are decided, the means for switching between ions must be considered. Any system for achieving this must be fast, reproducible, display very precise aiming and low "crosstalk" (i.e. overlap of the focal spot onto more than one ion), and be as simple as possible. In particular, it is desirable to be able to switch between different ions in the string in a time short compared to the time required to complete a given $\pi$-pulse on one ion. This tends to discount any sort of mechanical scanning system. Acousto-optic deflectors, which are often used for similar purposes, may be made fast enough, but introduce unwanted frequency shifts on the deviated beams. As a tentative solution, we propose to use an electro-optic beam deflector, basically a prism whose index of refraction, and consequently whose deflection angle, is varied slightly by applying a high voltage across the material; typical switching times for these devices is 10 nanoseconds, adequate for our purposes[9]. One such device produces a maximum deflection of $\pm 9$ mrad, for a $\pm 3000$V input. The associated maximum number of resolvable spots (using the Rayleigh criterion) is of order 100, implying that $\sim$ 20 ions could be comfortably resolved with negligible crosstalk.

After the inter-ion spacing has been determined, i.e., by the trap frequencies, the

[9] Note that while one could in principle control the pulse area merely by swinging the pulse on and off a given ion, the complications involved with exposing the ion to a varying spatial distribution make this undesirable.

crosstalk specification determines the maximum spot size of the addressing beam. For example, for an ion spacing of 20 $\mu$m, any spot size (defined here as the $1/e^2$ diameter) less than 21.6 $\mu$m will yield a crosstalk of less than 0.1%, assuming a purely Gaussian intensity distribution (a good approximation if the light is delivered from a single-mode optical fiber, or through an appropriate spatial filter). In practice, scattering and other experimental realities will increase this size, so that it is prudent to aim for a somewhat smaller spot size, e.g. 10 $\mu$m. One consideration when such small spot sizes are required is the effect of lens aberrations, especially since the spot must remain small regardless of which ion it is deflected on. Employing standard ray-trace methods, we have found that the blurring effects of aberrations can be reduced if a doublet/meniscus lens combination (figs.11.a) is used (assuming an input beam size of 3mm, and an effective focal length of 30mm). A further complication is that, in order to add or remove phonons from the system, the addressing beams must have a component along the longitudinal axis of the trap. Calculations indicate that an angle of only about $10^o$ between the pump beam and the normal to the ion string is sufficient for adequate coupling to the phonons. Nevertheless the addressing optics must accommodate a tilted line of focus, otherwise the intensity at each ion would be markedly different, and the crosstalk for the outermost ions would become unacceptable. According to ray-trace calculations, adding a simple wedge (of $\sim 2^o$) solves the problem (see Figs.11.b) and this has been confirmed by measurements using the mock system (Fig.11.c).

Depending on the exact level scheme being considered, it may be necessary to vary the polarization of the light (e.g., from left- to right-circularly polarized). Because the electro-optic deflector requires a specific linear polarization, any polarization-control elements should be placed after the deflector (see, for example, Fig. 10). The final result is a highly directional, tightly-focused beam with controllable polarization and intensity.

## 6.5 Imaging System

In order to determine the ions' locations and to readout the result of the quantum computations, an imaging system is required. Figure 12 shows our current imaging system, which consists of two lenses, one of which is mounted inside the vacuum chamber, and a video camera coupled to a dual-stage micro-channel plate (MCP) image intensifier. The first lens with focal length 15 mm collects the light emitted from the central trap region with a solid angle of approximately 0.25 sr. The image is relayed through a 110mm/f2 commercial camera lens to the front plate of the MCP. This set-

up produces a magnification of 7.5 at the input of the MCP. The input of the 110 mm lens is fitted with a 400nm narrow band filter to reduce background from the IR laser and from light emanating from the hot calcium oven and the electron gun filament.

The dual plate intensifier is operated at maximum gain for the highest possible sensitivity. This allows us to read out the camera at normal video rate of 30 frames $s^{-1}$ into a data acquisition computer. Averaging and integrating of the signal over a given time period can then be undertaken by software. We find this arrangement extremely useful in enabling us to observe changes of the cloud size or the intensity of the fluorescence with changes of external parameters like trapping potential, laser frequency, laser amplitude, etc. in real time.

The spatial resolution of the system is limited by the active diameter of individual channels of the MCP of approximately 12 $\mu$m. Since the gain is run at its maximum value cross talk between adjacent channels in the transition between the first and second stage is to be expected. This results in the requirement that two incoming photons can only be resolved when they are separated at the input of the MCP by at least two channels, i.e. by 36 $\mu$m in our case. With the magnification of the optical system of 7.5 this translates into a minimum separation of two ions to be resolved of 5 $\mu$m, which is well below the separation of ions in the axial well of about 25 $\mu$m expected in our experiment.

# 7 Summary and Conclusions

It is our contention that currently the ion trap proposal for realizing a practical quantum computer offers the best chance of long term success. This in no way is intended to trivialize research into the other proposals discussed in section 4: in any of these schemes technological advances may at some stage lead to a breakthrough. In particular, Nuclear Magnetic Resonance does seem to be a relatively straightforward way in which to achieve systems containing a few qubits. However, of the technologies which have so far been used to demonstrate experimental logic gates, ion traps seem to offer the least number of technological problems for scaling up to 10's or even 100's of qubits.

In this paper we have described in some detail the experiment we are currently developing to investigate the feasibility of cold trapped ion quantum computation. We should emphasize that our intentions are at the moment exploratory: we have chosen an ion on the basis of current laser technology, rather than on the basis of which ion which will give the best performance for the quantum computer. Other species of ion may

well give better performance: In particular, as mentioned in section 5, Beryllium ions do have the potential for a significantly lower error rate due to spontaneous emission, although it is also true that lighter ions may be more susceptible to heating. Other variations, such as the use of Raman transitions in place of single laser transitions, or the use of standing wave lasers need to be investigated. Our choice of Calcium will allow us to explore these issues. Furthermore, calculations suggest that it should be possible to trap 20 or more Calcium ions in a linear configuration and manipulate their quantum states by lasers on short enough time scales that many quantum logic operations may be performed before coherence is lost. Only by experiment can the theoretical estimates of performance be confirmed. Until all of the sources of experimental error in real devices are thoroughly investigated, it will be impossible to determine what ion and addressing scheme enables one to build the best quantum computer or, indeed, whether it is possible to build a useful quantum computer with cold trap ions at all.

# Acknowledgments

The authors would like to thank James Anglin, Howard Barnum, Rainer Blatt, Mark Bocko, Gavin Brennen, Carlton Caves, Ike Chuang, Ignacio Cirac, Ivan Deutsch, David DiVincenzo, Artur Ekert, Heidi Fearn, Salman Habib, Timothy Havel, Richard Jozsa, Hugh Klein, Manny Knill, Marvin Kruger, Norm Kurnit, Raymond Laflamme, Stephen Lea, Todd Meyrath, Chris Monroe, George Morgan, Keith Miller, Peter Milonni, Michael Neilsen, Albert Petschek, Martin Plenio, John Preskill, Bernard Rosen, Barry Sanders, Andrew Steane, David Wineland, Tanya Zelevinsky, Peter Zoller, and Wojciech Zurek for useful discussions and helpful comments. This research was funded by the National Security Agency.

# References

[1] R. J. Hughes, D. M. Alde, P. Dyer, G. G. Luther, G. L. Morgan and M. Schauer, Contemp. Phys. **36** (1995) 149-163.

[2] P. A. Benioff, Int. J. Theor. Phys.**21** (1982) 177-201.

[3] R. P. Feynman, Foundations of Physics **16** (1986) 507-531.

[4] D. Deutsch, Proc. R. Soc. Lond.**A 425** (1989) 73-90.

[5] D. Deutsch and R. Jozsa, Proc. R. Soc. Lond. **A 439** (1992) 553-558.

[6] D. Simon, *Proceedings of the 35th Annual Symposium on the Foundations of Computer Science*, S. Goldwasser ed., IEEE Computer Society Press, Los Alamitos CA, 1994, p.116

[7] P. W. Shor, *Proceedings of the 35th Annual Symposium on the Foundations of Computer Science*, S. Goldwasser ed., IEEE Computer Society Press, Los Alamitos CA, 1994.

[8] A. Ekert and R. Jozsa, Rev. Mod. Phys. **68** (1996) 733-753.

[9] J. I. Cirac and P. Zoller, Phys. Rev. Lett. **74**, (1995) 4094-4097.

[10] C. Monroe, D. M. Meekhof, B. E. King, W. M. Itano, and D. J. Wineland, Phys. Rev. Lett. **75** (1995) 4714-4717.

[11] E. Knill, R. Laflamme and W. Zurek, "Accuracy threshold for quantum computation"; submitted to *Science* (1997).

[12] J. Preskill, "Reliable quantum computers", preprint (1997), quant-ph/9705031.

[13] L. K. Grover *Proceedings of the 28th Annual ACM Symposium on the Theory of Computing*, ACM Press, New York, 1996 p.212

[14] B. M. Terhal and J. A. Smolin, " Superfast quantum algorithms for coin weighing and binary search problems", preprint (1997) quant-ph/9705041.

[15] D. Boneh and R. Lipton, "Quantum cryptanalysis of hidden linear functions," Proc. CRYPTO'95 (Springer, New York, 1995)

[16] A. Kitaev, "Quantum measurements and the Abelian stabilizer problem," preprint (1995) quant-ph 9511026.

[17] S. Lloyd, Scientific American (October 1995) 140-145.

[18] C. H. Bennet, IBM J. Res. Dev.**6** (1979) 525.

[19] E. Fredkin and T. Toffoli, Int J. Theor. Phys.**21** (1982) 219-253.

[20] R. J. Hughes and M. S. Neergaard, in preparation (1997)

[21] A. K. Lenstra and H. W. Lenstra, Lecture Notes in Mathematics 1554: The Development of the Number Field Sieve, (Springer, 1993).

[22] J. Cowie et al., "A world wide number field sieve factoring record: on to 512 bits", Advances in Cryptology-ASIACRYPT'96, pp 382 , K. Kim and T. Matsumoto eds. (Springer, New York , 1996).

[23] R. J. Hughes, D. F. V. James, E. H. Knill, R. Laflamme and A. G. Petschek, Phys. Rev. Lett. **77** (1996) 3240-3243.

[24] M. B. Plenio and P. L. Knight, Phys. Rev. **A 53** (1996) 2986-2990.

[25] S. Haroche and J.-M. Raimond, Physics Today (August 1996) 51-52.

[26] D. F. V. James, R. J. Hughes, E. H. Knill, R. Laflamme and A. G. Petschek, *Photonic Quantum Computing*, S. P. Hotaling, A. R. Pirich eds, *Proceedings of SPIE* **3076** (1997) 42-50.

[27] J. P. Schiffer, Phys. Rev. Lett. **70** (1993) 818-821.

[28] T. Pellizzari, S. A. Gardiner, J. I. Cirac and P. Zoller, Phys. Rev. Lett.**75** (1995) 3788-3791.

[29] Q. A. Turchette, C. J. Hood, W. Lange, H. Mabuichi and H. J. Kimble, Phys. Rev. Lett.**75** (1995) 4710-4713.

[30] P. Domokos, J.-M. Raimond, M. Brune and S. Haroche, Phys. Rev. **A 52** (1995) 3554-3557.

[31] R. Törmä and S. Stenholm, Phys. Rev.**A 54** (1996) 4701-4706.

[32] D. G. Cory, A. F. Fahmy and T. F. Havel, Proc. Natl. Acad. Sci. USA **94** (1997) 1634-1639.

[33] N. A. Gershenfeld and I. L. Chuang, Science **275** (1997) 350-356.

[34] D. G. Cory, A. F. Fahmy and T. F. Havel, *Proc. 4th Workshop on Physics and Computation*, T. Toffoli, M. Biafore and J. Leão eds. (1986) pp. 87-91. Seminar given by T. F. Havel at Los Alamos National Laboratory, 30 May 1997.

[35] W. S. Warren, "Can bulk spin-resonance quantum computation ever be useful?", Science (1997) in the press.

[36] J. R. Friedman, M. P. Sarachik, J. Tejada and R. Ziolo, Phys. Rev. Lett. **76** (1996) 3830-3833.

[37] D. P. DiVincenzo, Phys. Rev. **A 51** (1995) 1015-1022.

[38] V. Privman, I. D. Vagner and G. Kventsel, "Quantum computation in quantum-Hall systems", preprint (1997), quant-ph/9707017.

[39] R. Rouse, S. Y. Han and J. E. Lukens, Phys. Rev. Lett.**75** (1995) 1614-1617.

[40] M. F. Bocko, A. M. Herr and M. J. Feldman, "Prospects for quantum coherent computation using superconducting electronics", preprint (1997).

[41] B. Rosen, "Superconducting circuit implementation of qubits and quantum computer logic", preprint (1997).

[42] A. Barenco, D. Deutsch, A. Ekert and R. Jozsa, Phys. Rev. Lett. **74** (1995) 4083-4086.

[43] D. Loss and D. P. DiVincenzo, "Quantum computation with quantum dots" preprint (1997), cond-mat/9701055.

[44] A. M. Steane, Applied Physics **B 64** (1997) 623-642.

[45] D. J. Wineland, C. Monroe, W. M. Itano, D. Leibfried, B. E. King and D. M. Meekhof, "Experimental issues in coherent quantum-state manipulation of trapped atomic ions", to be submitted to Rev. Mod. Phys. (1997).

[46] C. Monroe, D. M. Meekhof, B. E. King, S. R. Jefferts, W. M. Itano, D. J. Wineland and P. Gould, Phys. Rev. Lett. **75** (1995) 4011-4014.

[47] R. P. Feynman, F. L. Vernon and R. W. Hellwarth, J. Appl. Phys. **28** (1957) 49-51.

[48] L. Allen and J. H. Eberly, *Optical Resonance and Two-Level Atoms* Dover Books 1986.

[49] D. F. V. James, "Quantum dynamics of cold trapped ions, with application to quantum computation", Applied Physics B, in the press (1997).

[50] A. Schenzle and R. G. Brewer, Phys. Rep. **43** (1978) 455-484.

[51] G. Brennen and D. F. V. James, "The theory of Raman processes in Cirac-Zoller quantum computers", preprint, 1997.

[52] C. Monroe, D. Leibfried, B. E. King, D. M. Meekhof, W. M. Itano and D. J. Wineland, Phys. Rev. **A 55** (1997) R2489.

[53] E. T. Jaynes and F. W. Cummings, Proc. I.E.E.E. **51** (1963) 89.

[54] J. I. Cirac, R. Blatt, P. Zoller and W. D. Phillips, Phys. Rev. **A 46** (1992) 2668-2681.

[55] P. W. Milonni and J. H. Eberly, *Lasers* Wiley, 1988.

[56] M. Roberts, P. Taylor, G. P. Barwood, P. Gill, H. A. Klein and W. R. C. Rowley, Phys. Rev. Lett. **78** (1997) 1876-1879.

[57] G. Morgan, private communication, 1997.

[58] A. M. Steane, private communication, 1996.

[59] R. Blatt, private communication, 1997.

[60] W. Paul and H. Steinwedel, Z. Naturforsch.**A 8** (1953) 448.

[61] M. G. Raizen, J. M. Gilligan, J. C. Bergquist, W. M. Itano and D. J. Wineland, Phys. Rev. **A 45** (1992) 6493-6501.

[62] P. K. Ghosh, *Ion Traps* Clarendon Press, 1995.

[63] F. Diedrich, J. C. Bergquist, W. M. Itano and D. J. Wineland, Phys. Rev. Let. **62** (1989) 403-407.

[64] M. Abramowitz and I. A. Stengun, *Handbook of Mathematical Functions* Dover Books, 1965, chapter 20, p.721 ff.

[65] R. Blatt and C. Naegerl, private communication.

[66] S. K. Lamoreaux, "Thermalization of trapped ions: a quantum perturbation approach", submitted to Phys. Rev. A (1997).

[67] D. J. Wineland and H. G. Dehmelt, J. Appl. Phys. **46** (1975) 919-930.

[68] D. J. Wineland, J. Bollinger, W. Itano and D. Heinzen, Phys. Rev. **A 50** (1994) 67-88.

[69] S. Stenholm, Rev. Mod. Phys. **58** (1986) 699-739.

[70] D. J. Wineland and W. M. Itano, Phys. Rev.**A 20** (1979) 1521-1540.

[71] M. B. Plenio, private communication (1996).

# Figure Captions

Figure 1. A schematic illustration of an idealized laser-ion interaction system; $\mathbf{k}_L$ is the wavevector of the single addressing laser.

Figure 2. The lowest energy levels of $^{40}Ca^+$ ions, with transition wavelengths and lifetimes listed. See [49] for references to the data.

Figure 3. A schematic illustration of (a) single laser and (b) Raman qubit addressing and control techniques.

Figure 4 (a) Side view diagram of the linear RF trap used to confine $Ca^+$ ions in these experiments. The endcap separation is 10 mm and the gap between the RF rods is 1.7 mm. (b) End-on view of the linear RF trap electrodes.

Figure 5 (a) Photograph of the trap assembly (b) Photograph of the assembled ion trap vacuum system.

Figure 6. Image of a trapped Calcium ion

Figure 7. Calculated minimum ion separation as a function of axial oscillation frequency for $Ca^+$ ions in a harmonic well. The frequency is proportional to the applied endcap bias voltage and is dependent on the trap geometry.

Figure 8. Frequency of the axial motion of an ion cloud in the linear RF trap. The diamonds are the data points measured by resonant excitation which are to be compared to the results of an early model calculation for our geometry (solid circles). The line is a fit to a quadratic relation between frequency and voltage, the proportionality factor gives the effective strength of the axial potential due to the shielding by the RF rods.

Figure 9. Different transitions between the levels of $Ca^+$ ions required for (a) Doppler cooling, (b) Resolved sideband cooling and (c) quantum logic operations and readout. The single laser addressing technique has been assumed.

Figure 10.Illustration of the laser beam control optics system.

Figure 11. Ray trace diagram of the laser beam control optics in the focal region; a) doublet meniscus wedge optics for ion addressing; b) ray-trace diagram in the focal region, showing the ability of the system to address individual ions; c) normalized profile from an experimental test of addressing optics, using a 670nm diode laser and a 5 $\mu$m diameter scanning pinhole. In this case the maximum cross talk was 0.34%.

Figure 12. Illustration of the ion imaging system.

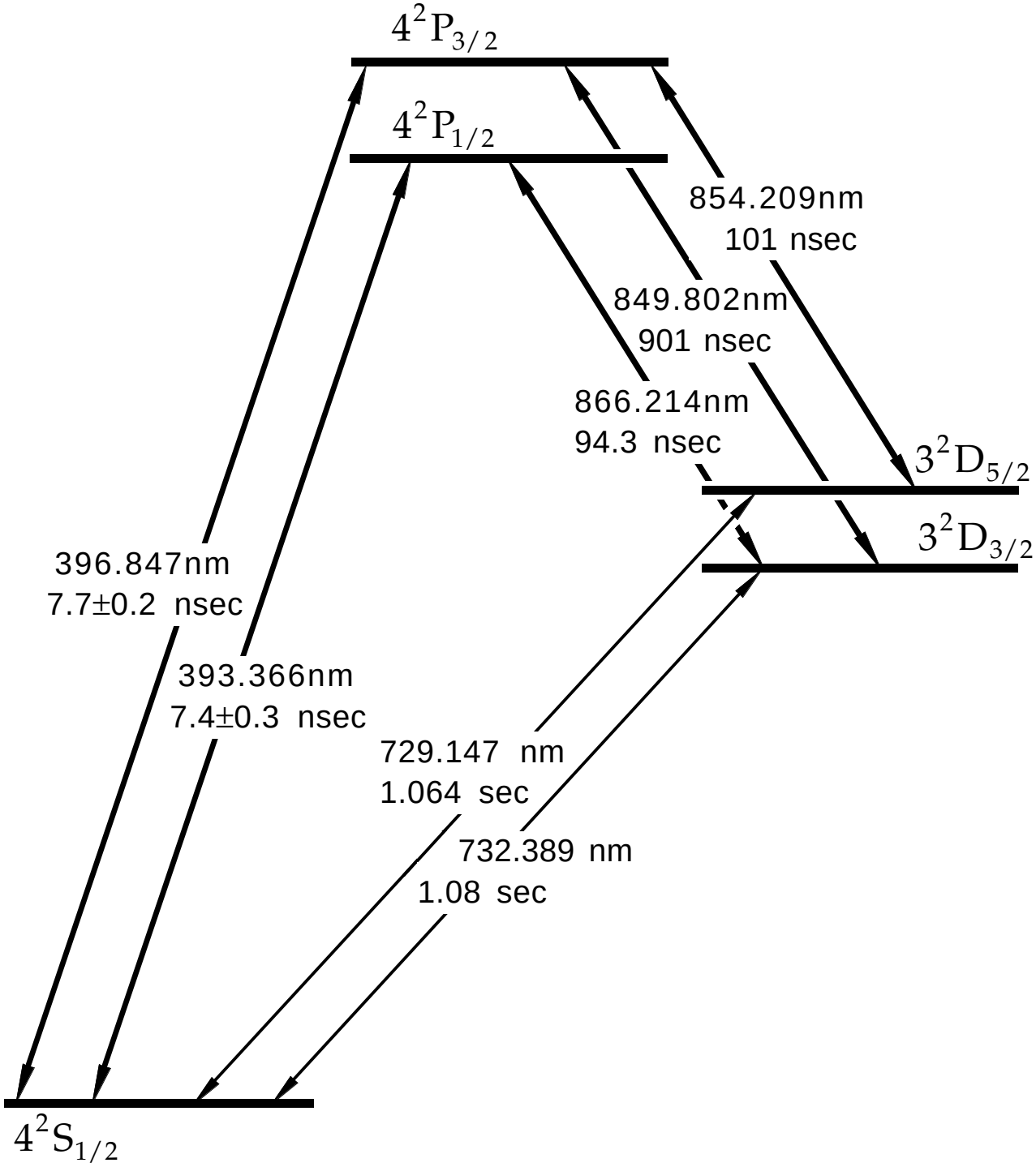

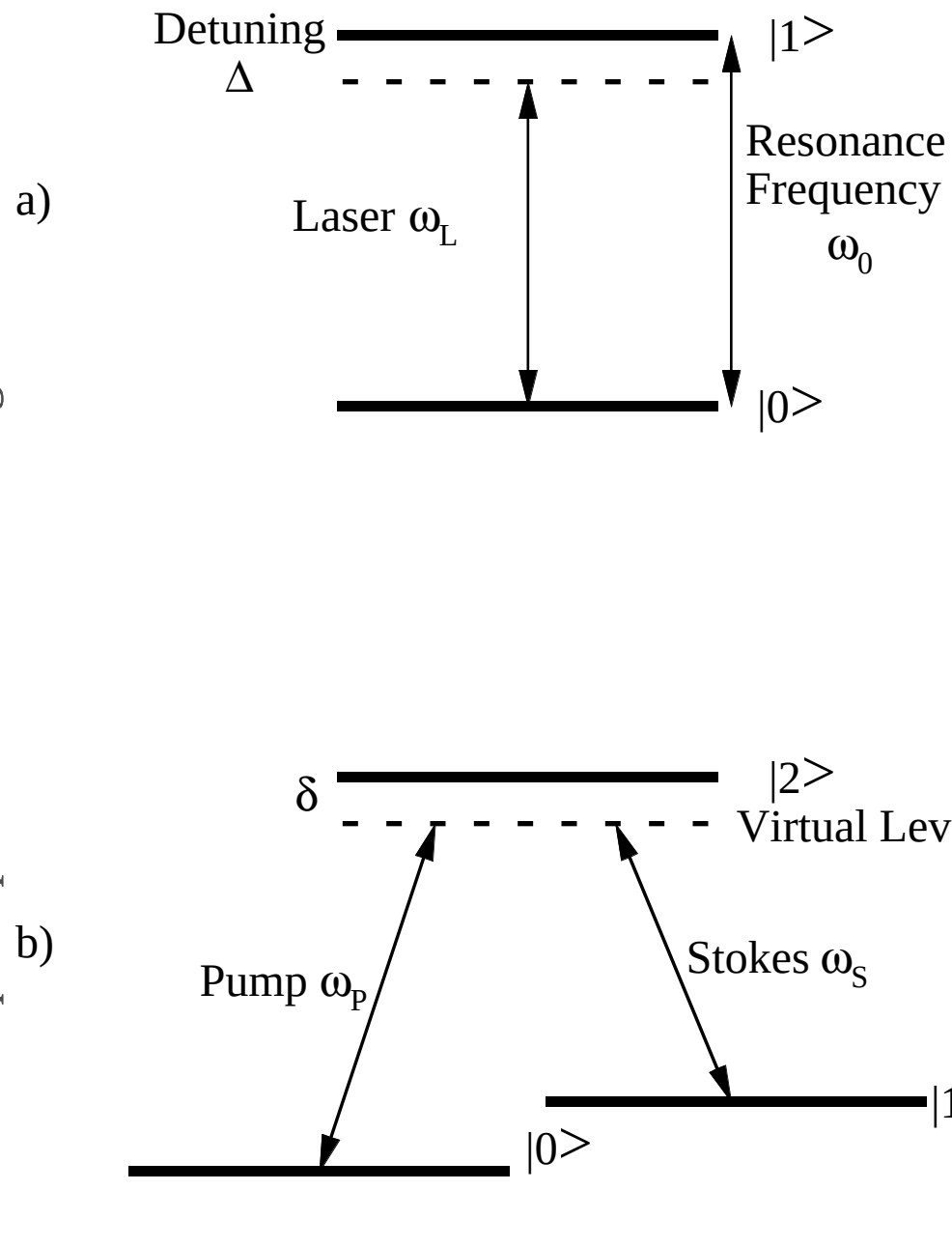

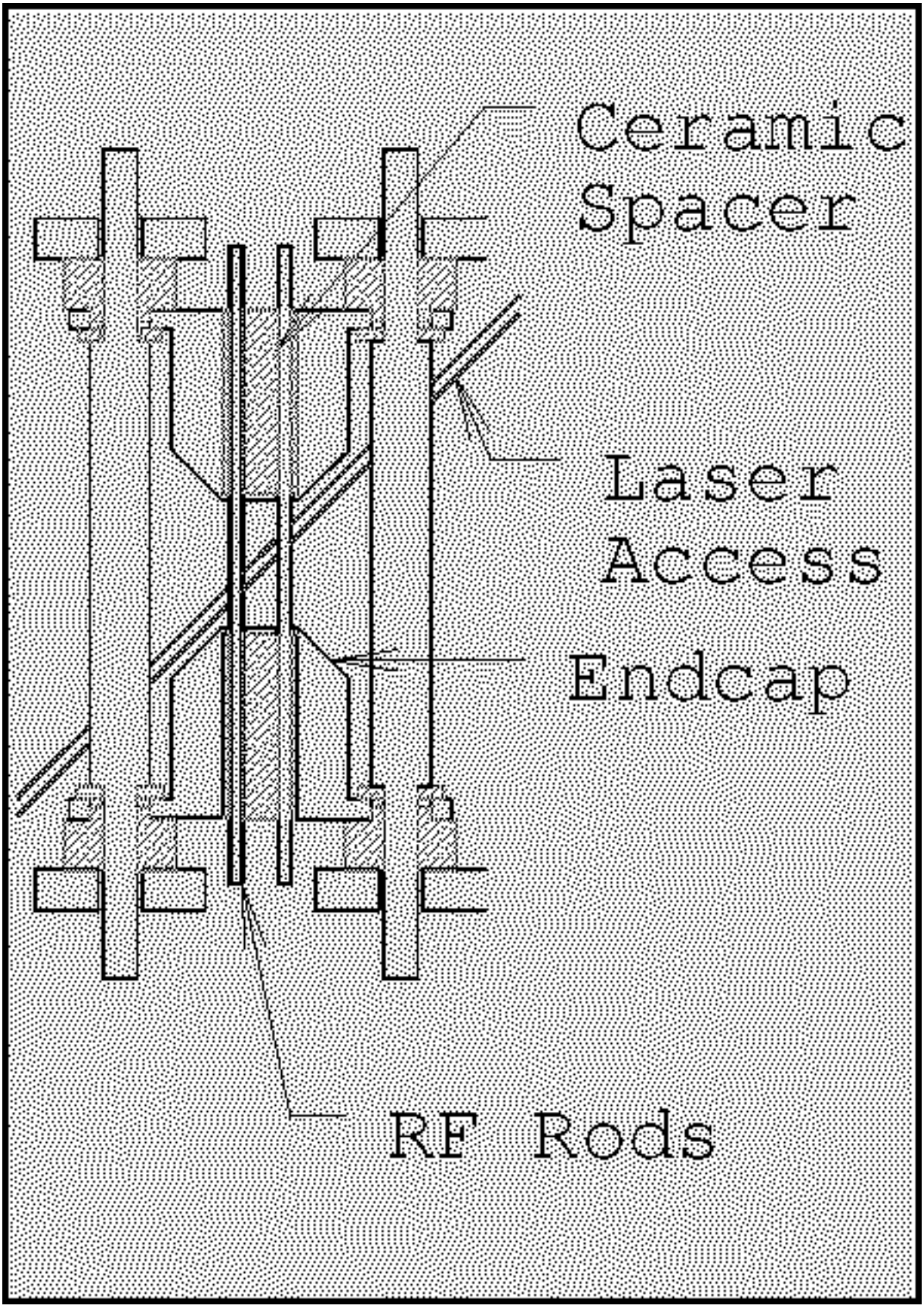
Ceramic
Spacer
Laser
Access
Endcap
RF Rods

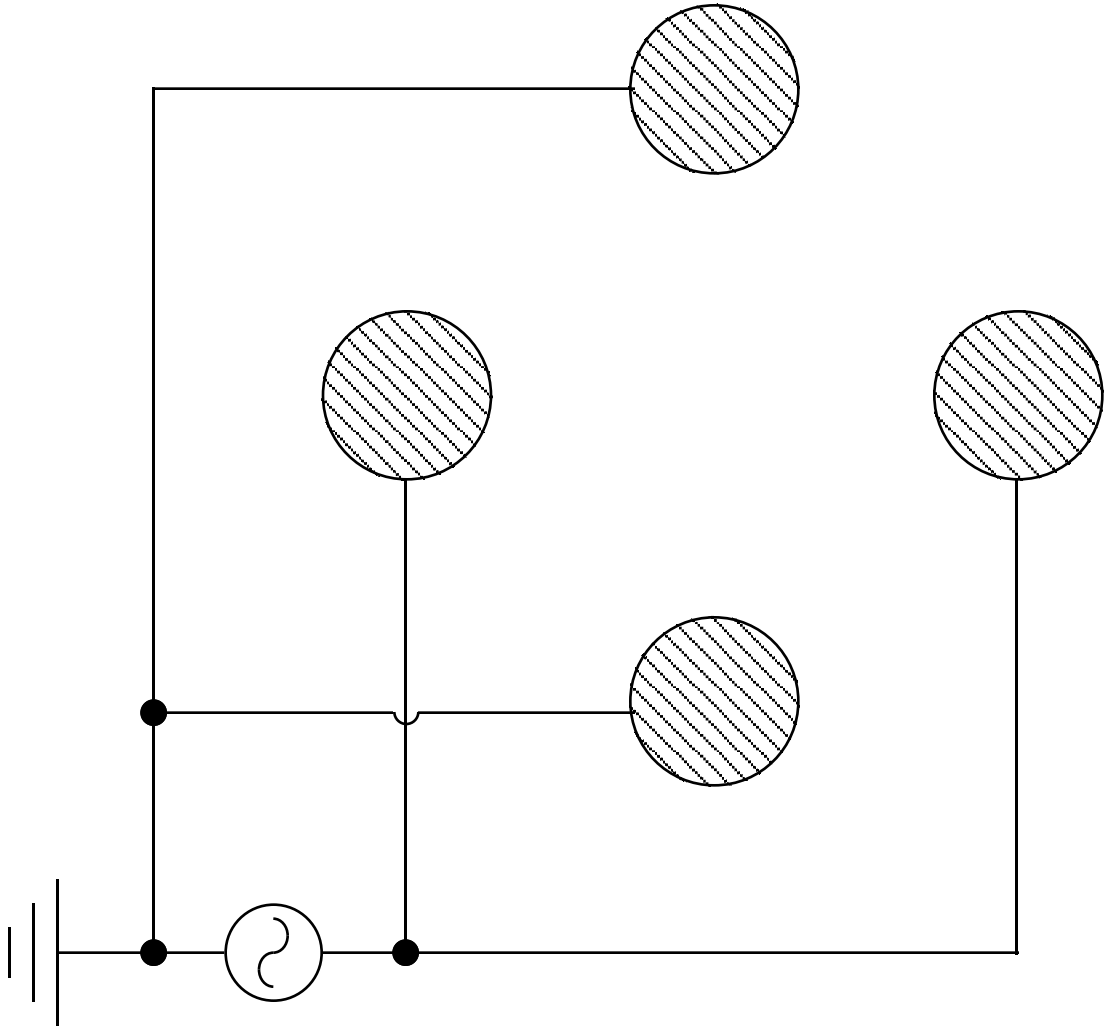

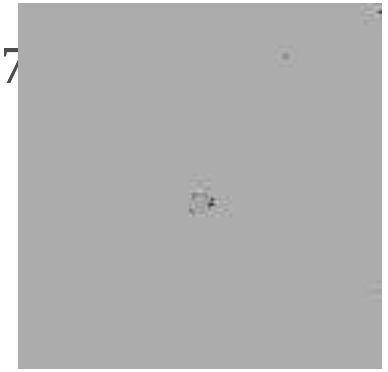

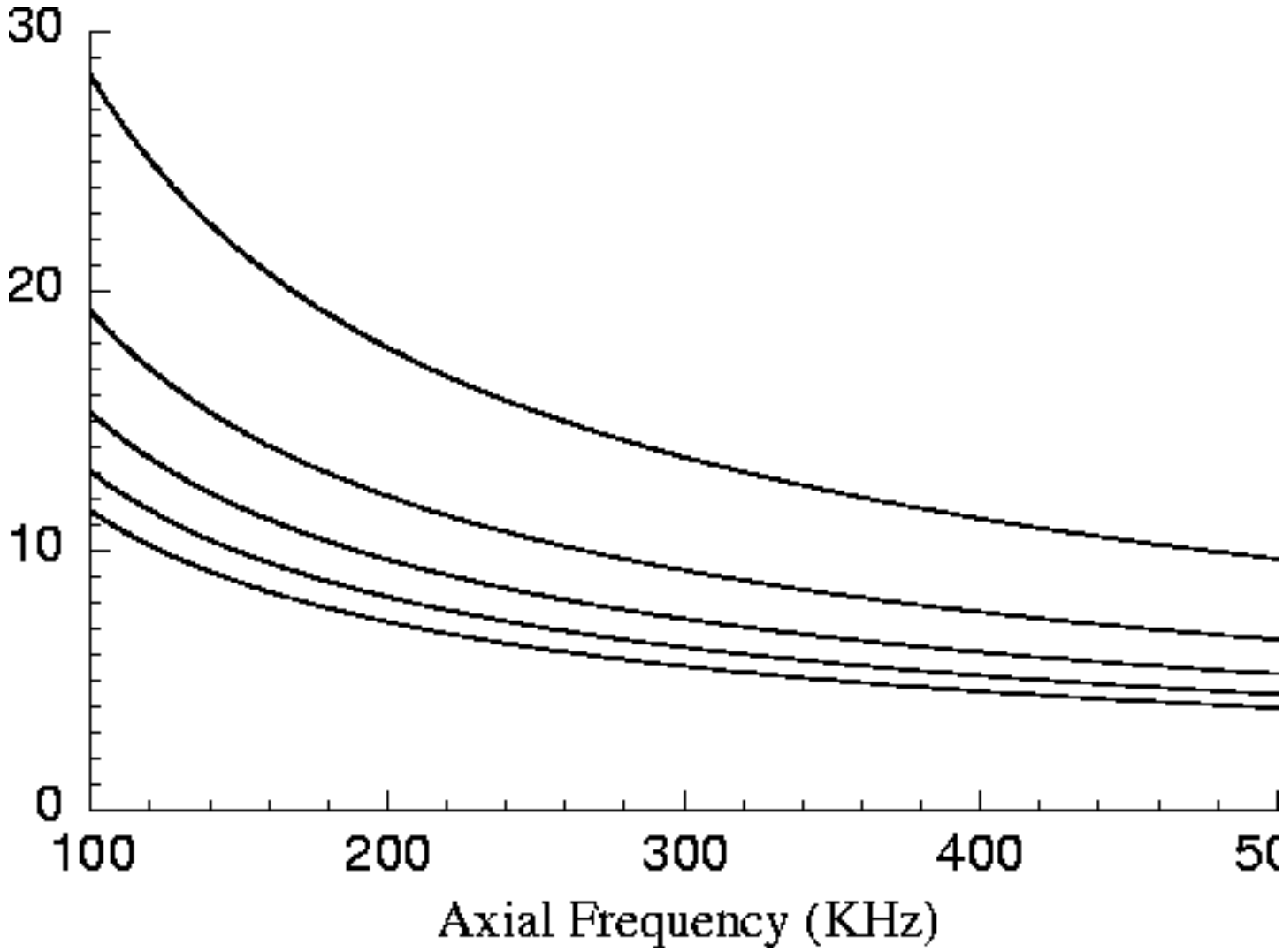
30
20
10
0
100
200
300
400
Axial Frequency (KHz)

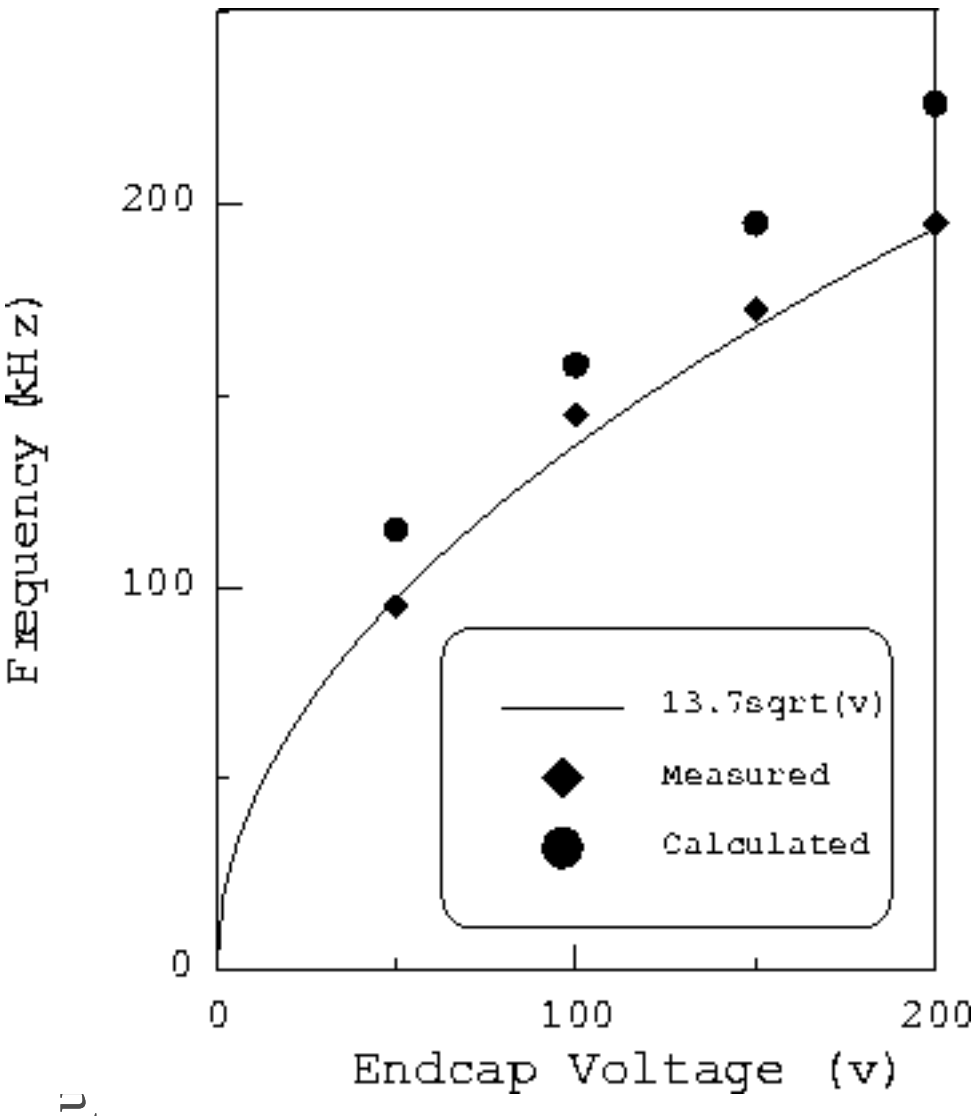
Frequency (kHz)
200
100
0
0
100
200
Endcap Voltage (v)
13.7sqrt(v)
Measured
Calculated

a)

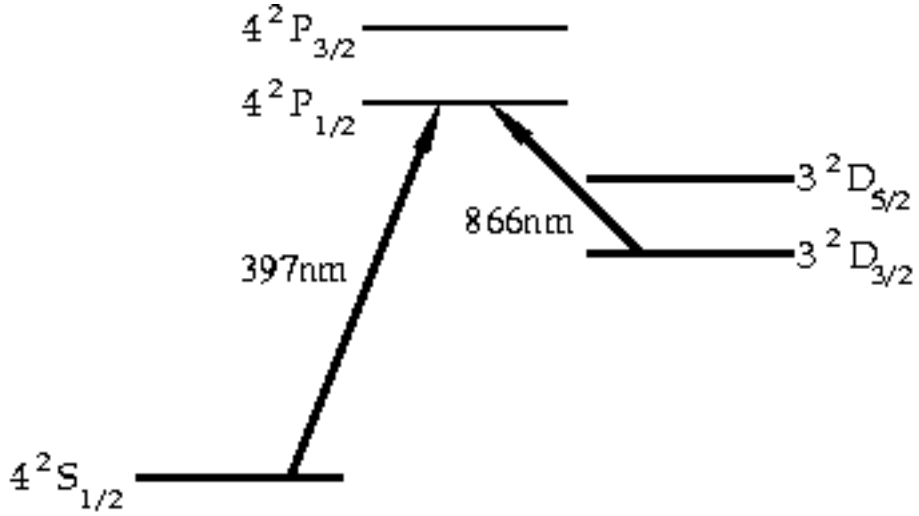
$4^2P_{3/2}$
$4^2P_{1/2}$
$3^2D_{5/2}$
866nm
$3^2D_{3/2}$
397nm
$4^2S_{1/2}$

b)

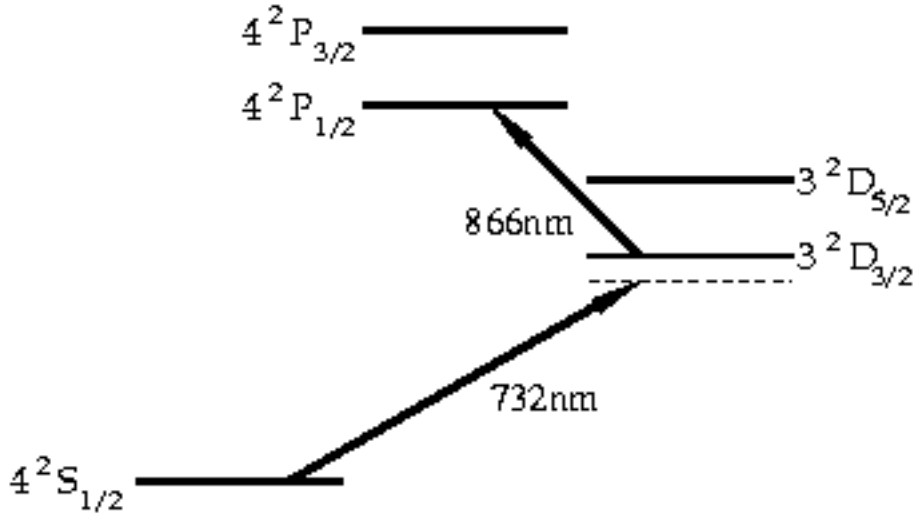
$4^2P_{3/2}$
$4^2P_{1/2}$
$3^2D_{5/2}$
866nm
$3^2D_{3/2}$
732nm
$4^2S_{1/2}$

c)

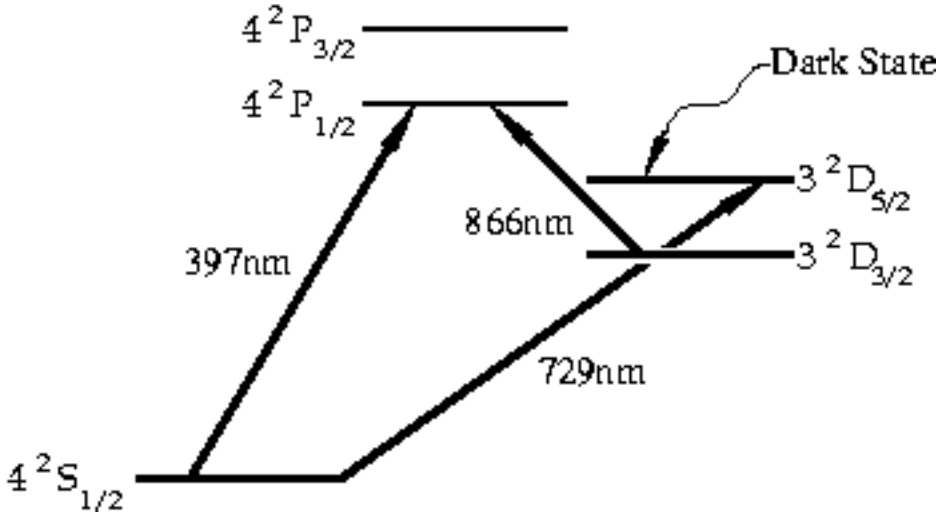
$4^2P_{3/2}$
Dark State
$4^2P_{1/2}$
$3^2D_{5/2}$
866nm
$3^2D_{3/2}$
397nm
729nm
$4^2S_{1/2}$

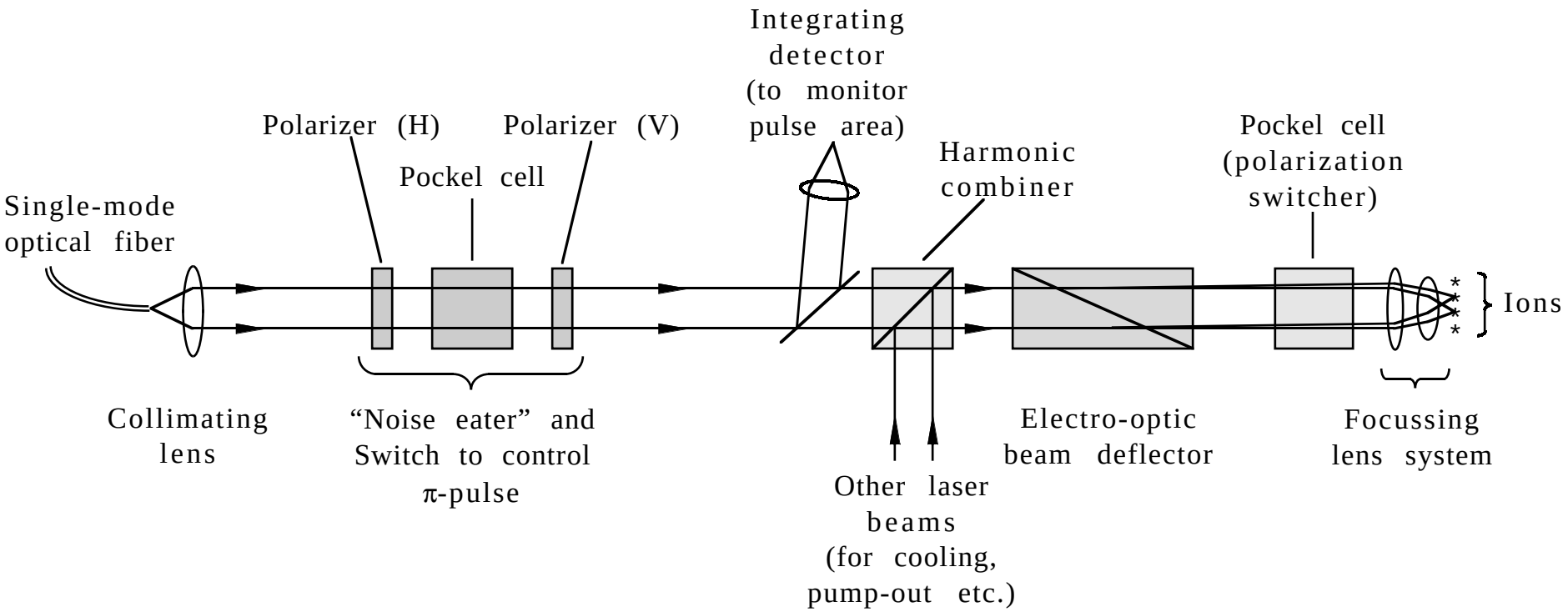

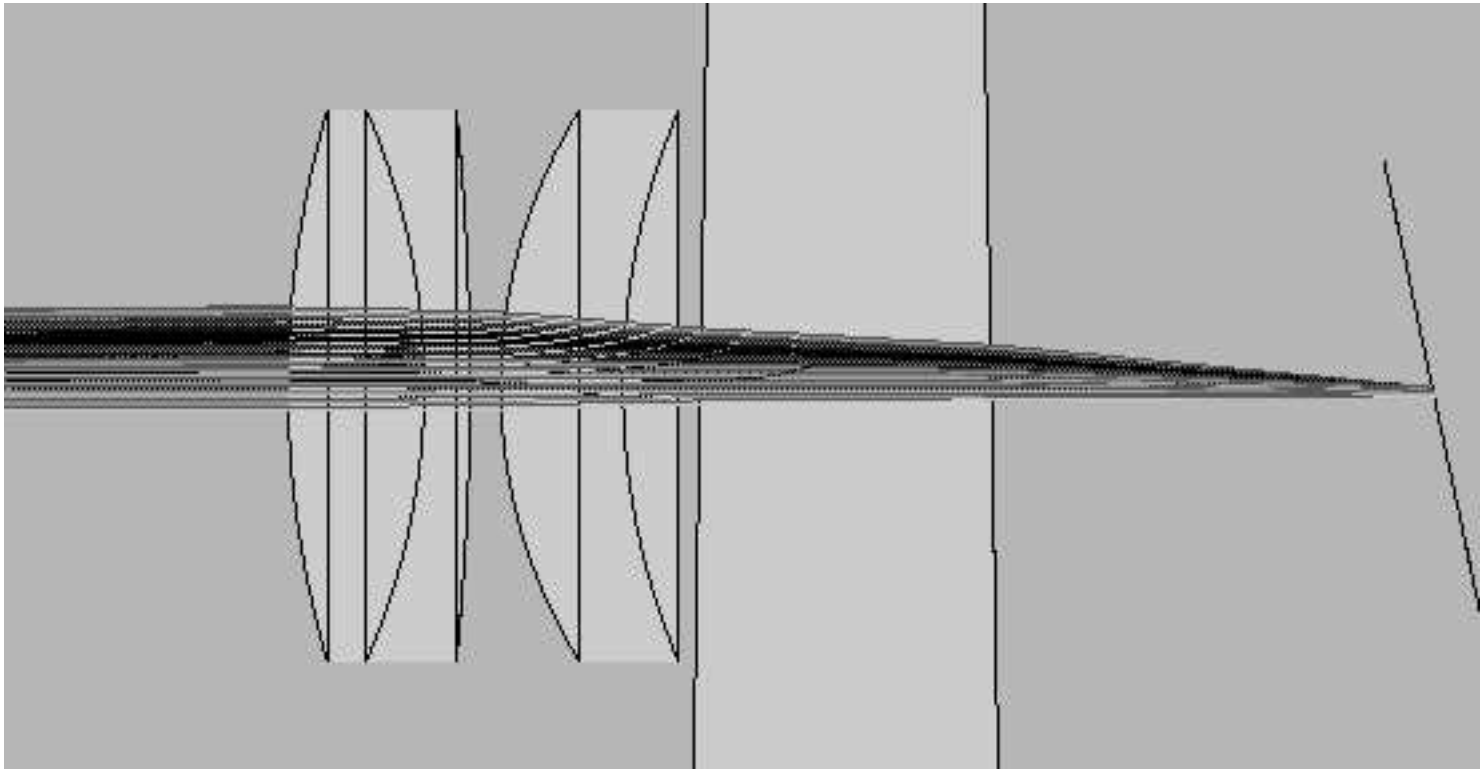

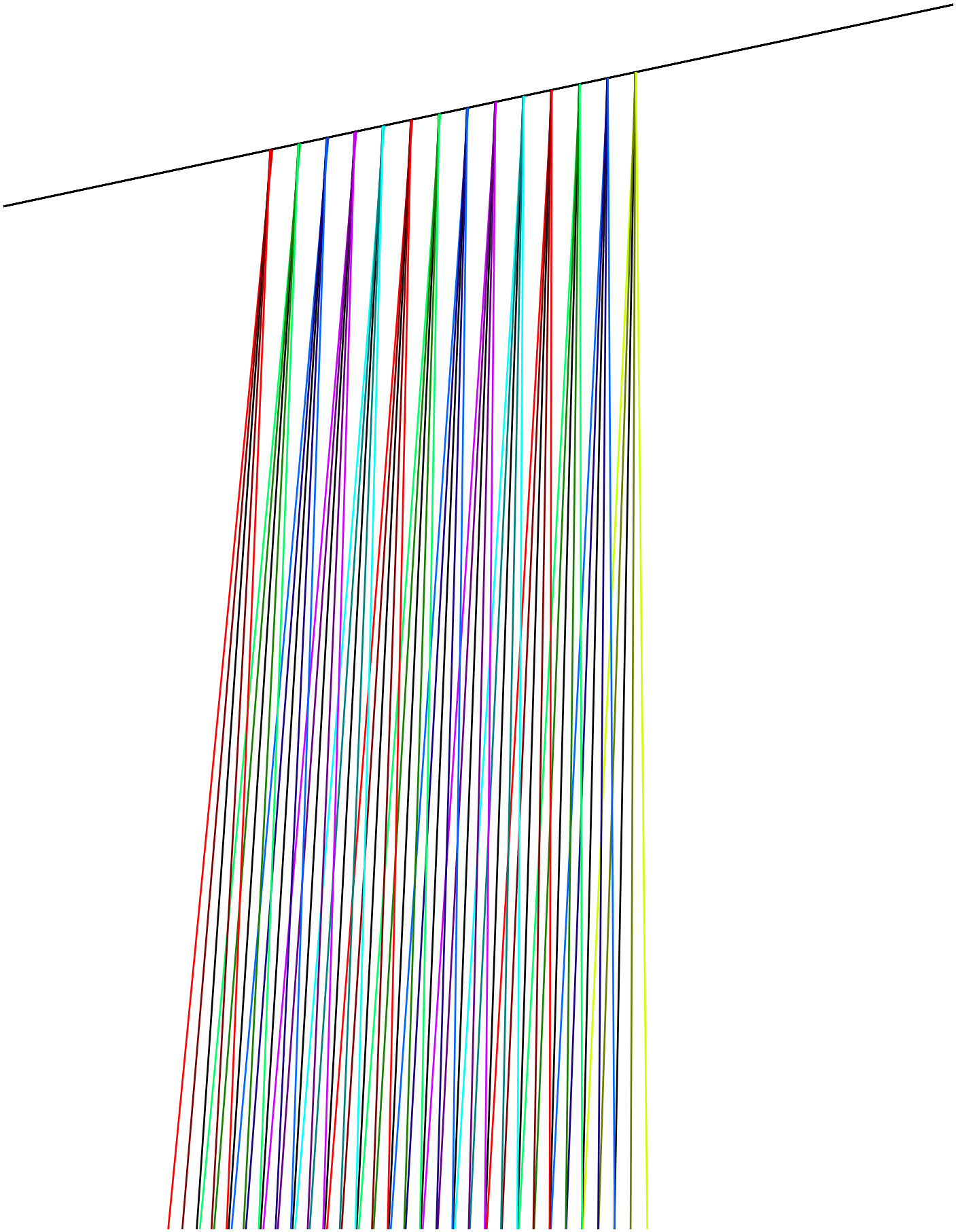

Normalized Power
0
0.2
0.4
0.6
0.8
1
-80
-40
0
40
Position (μm)